ATMOSPHERIC HOLES AND SMALL COMETS

L. A. Frank and J. B. Sigwarth

Department of Physics and Astronomy
University of Iowa
Iowa City

Abstract. Global images of Earth's ultraviolet dayglow as gained with an imaging photometer on board Dynamics Explorer 1 exhibit transient decreases, or atmospheric holes, in the dayglow intensities over areas with diameters ~50 km. Features of these atmospheric holes include (1) preferential motion in the east-to-west direction across the sunlit face of Earth, (2) similar diurnal variations in occurrence rates as those for radar meteors, (3) correlation of the occurrence rates with the nonshower rates as determined with forward scatter radar, and (4) larger angular diameters for these atmospheric holes when the spacecraft approaches Earth during its perigee passes. A significantly less extensive series of images of Earth's ultraviolet dayglow with the Viking spacecraft also provides evidence of these atmospheric holes. The atmospheric holes are interpreted in terms of obscuration of the dayglow by water clouds from the disruption and subsequent vaporization of small comets at low altitudes above the atmosphere. Supporting evidences for the existence of these small comets are given by telescopic sighting of these objects at greater altitudes before disruption and the detection of water bursts in Earth's upper atmosphere. We summarize the current status of this small-comet hypothesis and its relationship to conventional wisdom concerning geophysical, lunar, and interplanetary phenomena.

1. INTRODUCTION

A spin-scan imaging photometer for ultraviolet wavelengths is included in the instrumentation for the Dynamics Explorer 1 spacecraft [*Frank et al.* 1981]. This spacecraft circumnavigates Earth in an eccentric polar orbit with initial inclination of 90°, perigee and apogee altitudes of 570 km and 3.65 R_E (Earth radius), respectively, and an orbital period of 6.83 hours at launch on August 3, 1981. The primary scientific purpose of the imaging photometer is to obtain global images of the auroral zones [cf. *Frank and Craven,* 1988]. Global images of the ultraviolet dayglow are also available. An example of such an image is shown in Plate 1 [*Frank et al.,* 1986*g*]. This image is primarily a record of emissions from the multiplets of atomic oxygen at 130.4 and 135.6 nm. Two atmospheric holes, or regions of transient intensity decreases, in the dayglow are shown in the inset of Plate 1. The smaller atmospheric hole occurs in one pixel of the image, the other atmospheric hole is tracked in two consecutive vertical scan lines each separated by the 6-s spin period of the spacecraft.

These atmospheric holes are interpreted by *Frank et al.* [1986*b*] as the result of water clouds that are absorbing the atmospheric dayglow along the light of sight to the spacecraft. The water clouds are the vaporized water snows of the cores of small comets that are disrupted at low altitudes above Earth's atmosphere. The corresponding global influx of these small comets is about 20/min from the occurrence rate of atmospheric holes and the mass of each comet is $\sim 10^8$ g, i.e., the amount of water vapor required to absorb the ultraviolet dayglow over an area with diameter ~50 km at altitudes above the dayglow layer, $\gtrsim$ 300 km. Recent detection of the small comets before their disruption at low altitudes with a ground-based telescope provides a better estimate for the typical small-comet mass, ~2 x 10^7 g [*Yeates,* 1989; *Sigwarth,* 1989; *Frank et al.,* 1990*b*].

Dessler [1991] summarizes the current arguments against the existence of atmospheric holes and a large population of small comets in the inner solar system. Because an extensive variety of topics is discussed, we organize our responses in the same order as given by *Dessler* [1991] for the purposes of clarity for the reader. The reader may gain considerable insight into the controversy concerning atmospheric holes and small comets by comparative readings, section by section, of the paper by *Dessler* [1991] and the following responses.

2. DISRUPTION, VAPORIZATION, AND EVENT RATE

The rates of small-comet impacts into Earth's atmosphere as inferred from observations of atmospheric holes with the Dynamics Explorer 1 ultraviolet imager are similar to the rates obtained from direct telescopic detection (see section 5.2.1.) and from a survey of bursts of microwave radiation from water in the upper atmosphere (see section 3). On the other hand, the telescopic measurements indicate that the typical mass is significantly less than the 10^8 g originally proposed by *Frank et al.* [1986*b*] that is necessary to absorb the ultraviolet dayglow by molecular water over a circular area with radius ~ 25 km. The telescopic observations indicate a typical mass of ~2 x 10^7 g, i.e., too small to account for the observed dayglow absorption.

Reviews of Geophysics, 31, 1 / February 1993
pages 1 -28
8755-1209/93/92RG-02316 $15.00
Paper number 92RG02316

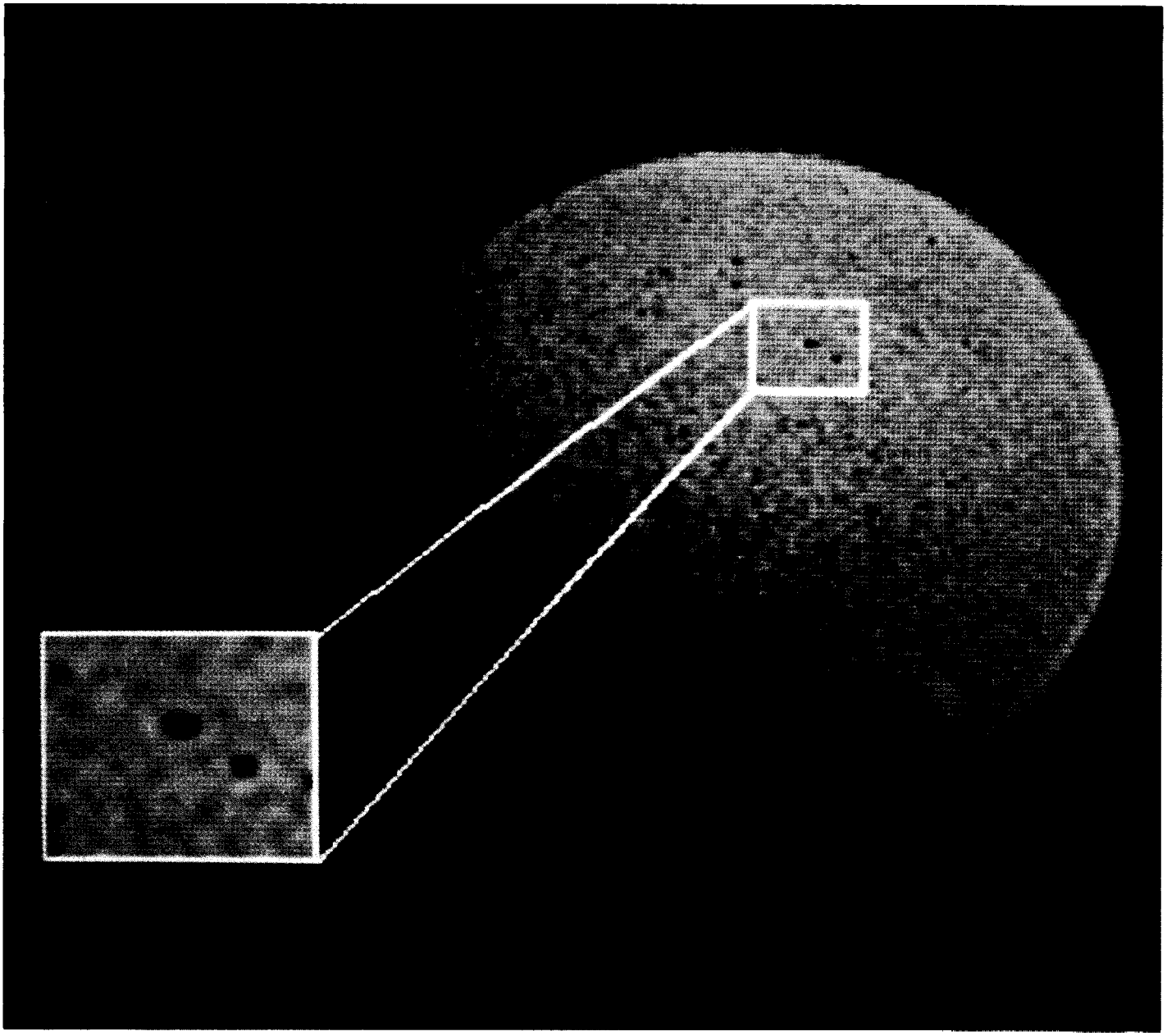

Plate 1. Image of Earth's ultraviolet dayglow, primarily in the atomic oxygen emissions at 130.4 nm, as taken with a spin-scan photometer on hoard Dynamics Explorer 1. An atmospheric hole that is detected in two consecutive scan lines is shown near the center of the inset, along with evidence of a bright feature in the next scan line, as the photometer's scanning mirror tracks the object. The other atmospheric hole in the inset is seen only in one scan line. This image is taken from altitude 23,000 km and geographic latitude and longitude ~ 48° and 35°, respectively, at 0709 UT on October 10, 1982 [after *Frank et al.,* 1986*g*].

Our original estimate for the mass of a small comet is based upon the assumption that the water cloud primarily comprises the monomer form of water, $(H_2O)_1$. The total absorption cross section for this monomer at the wavelength of primary interest is ~5 x 10^{-18} cm^2 at 130.4 nm [*Watanabe and Zelikoff,* 1953]. A. L. Lane (private communication, 1991) brings to our attention that the expanding cloud of water vapor from the small comet can provide an environment in which water dimers, $(H_2O)_2$, or clusters, $(H_2O)_n$, can be formed. The presence of water dimers in the outflowing vapors from comet P/Halley is suggested by *Murad and Bochsler* [1987] in order to account for the large amounts of H_3O^+ observed in this comet's coma. The reader is referred to the paper by *Berry* [1990] for an overview of the structure and dynamics of dimers and clusters. Formation of water dimers by gas nozzle expansion in the laboratory is discussed by

Dyke et al. [1977] and *Odutola and Dyke* [1980]. Water clusters are also produced by such laboratory apparatus [*Duke and Muenter,* 1972]. In the weakly hydrogen-bonded dimer the O–O internuclear distance R_{oo} is 3.0 A, and, for comparison, the O-H equilibrium bond length is 0.96 Å [*Dyke et al.,* 1977].

It is not unreasonable to assume that the undisrupted contents of these small comets may arise from the accretion of water clusters into a water frost or snow in the distant Oort disk under conditions of very low densities and temperatures. The water clusters can be considered as very small ice crystals because the binding forces are the same. Relative speeds for quasi-circular, prograde orbits are small at these heliocentric radial distances. For example, the collisional speed of two objects, one in circular orbit at 10,000 AU and the other in an eccentric orbit with perihelion at 9000 AU and aphelion at 10,000 AU,is only about 800 cm/s, or ~6 x 10^{-6} eV/H_2O molecule, well below the sublimation energy for water snow of 0.49 eV as cited by *Delsemme and Miller* [1971]. Thus catastrophic collisional disruption or compaction is not expected and the formation of low-density, small comets in the Oort disk can be anticipated.

The ultraviolet absorption cross section per water molecule for the molecular water clusters may exceed that of the monomer. If so, then the cometary water mass necessary to produce an atmospheric hole as seen by Dynamics Explorer 1 is correspondingly less. Our search of the literature reveals no available data on the absorption cross section for water dimers or clusters in the wavelength range ~100 to 200 nm. However, *Shardanand* [1967] reports the absorption cross section for the Xe dimer at 121.6 nm. This wavelength does not correspond to a resonance line of atomic Xe. The absorption cross section is -5 x 10^{-22} cm² for Xe and increases to 1.85 x 10^{-17} cm² for Xe

In order to account for the absorption of 0 I 130.4-nm emissions for an atmospheric hole by a cometary water mass of 2 x 10^7 g, only a relatively modest increase of cross section is required for the water dimer $(H_2O)_2$ relative to the monomer H_2O. Specifically, the cross section per H_2O molecule in the dimer is required to be ~3 x10^{-17} cm², a factor of ~6 larger than that for monomer H_2O. Such cross sections are consistent with those for the dimer Xe_2 and considerably smaller than that for the geometric cross section of the dimer $(H_2O)_2$, ~3 x10^{-16} cm². We assume that the absorption cross section for each bond in a cluster of n molecules, $(H_2O)_n$, is similar. Laboratory measurements are required to confirm these inferences from the Xe_2 cross sections observed by *Shardanand* [1967].

Thus on the basis of the best estimate for the typical cometary mass from the telescopic observations we propose that the cometary water clouds are primarily composed of water dimers and clusters.

2.1. Breakup of a Small Comet

In their original paper, *Frank et al.* [1986*b*] suggest three possible forces for the disruption of small comets at low altitudes: (1) tidal, (2) electrostatic, and (3) ram pressures. The atmospheric ram forces are small relative to the gravitational tidal forces and no estimate of the electrostatic forces is given by these authors. *Frank et al.* [1986*b*] note that the tidal stresses at an altitude of 1700 km are ~0.1 dyne/cm². *Dessler* [1991] miscites this value as ~5 x 10^{-4} dyne/cm². This latter value is the surface gravitational pressure on a small comet that is used by *Frank et al.* [1986*b*, p. 308] "in lieu of any other bench mark for the binding forces in cometary material."

In response to the later criticisms by *McKay* [1986] concerning the thermal stability of small comets at 1 AU, *Frank et al.* [1986*e*] find that the small comets are marginally stable, i.e., temperatures are near the melting point of water snow, if the assumption is made that the water snow core is at the same temperature as the surface of the carbon mantle. The corresponding water vapor pressure at the mantle-core interface is ~ 5 x10^3 dyne/cm². Clearly, this assumption is inadequate except for a rough estimate of the upper limit for the vapor pressures within the small comet that must be restrained by the tensile strength of the carbon mantle. A more realistic model of heat transport within the small comet must be used in order to estimate the range of water vapor pressures at the mantle-core interface. Accordingly, the comet model of *Fanale and Salvail* [1984] is employed in order to numerically solve the heat transport equations (see section 4.2) for the mantle-core temperature. For carbon dust mantles with thicknesses 1, 2, and 3 cm the corresponding water vapor pressures are ~0.2, 2 x10^{-3}, and 2 x 10^{-4} dyne/cm², respectively, at 1 AU. These water vapor pressures give orders of magnitude lower limits for the tensile strength of the carbon mantle but cannot be used as measures of the mantle tensile strength; i.e., the tensile strength may be much greater than these vapor pressures. For comparison, the tensile strength of fresh, powdery snow at Earth's surface is ~5 x10^4 dyne/cm² [*Dorsey,* 1940].

The atmospheric ram pressures at altitudes ~1000 km are ~10^{-5} dyne/cm² and are probably too small for disruption of the small comets. The tidal stresses at these altitudes, ~0.1 dyne/cm², are in the range of the water vapor pressures constrained by the mantle as noted above. However, the radial dependence of these stresses varies as r^{-3}, where r is the geocentric radial distance and does not yield a rapid increase in stress over spatial scales of ~100 to 1000 km. Of the three disruptive forces originally identified by *Frank et al.* [1986*b*], electrostatic forces appear to be the most likely mechanism for removal of the protective mantle at altitudes ~1000 km.

The electrostatic stress on a smooth sphere with diameter of 12 m and at a potential of V_0 = 10 V is show in Figure 1 as a function of altitude above the Earth's surface. This value for V_0 is chosen because it is scalewise representative of the potential due to -V x B electric fields at the ionospheric altitudes, which are of primary interest here. The stress is $|\mathbf{E}_0|^2/8\pi$, where $\mathbf{E}_0$ is the electric field at the mantle surface. At altitudes beyond the plasmasphere the electrostatic screening thickness, or Debye length λ_D, in the ambient

plasma is large relative to the radius R_0 of the small comet and thus $|\mathbf{E}_0| \simeq V_0/R_0$. As λ_D decreases with decreasing altitude inside of the plasmapause, $|\mathbf{E}_0| \simeq V_0/\lambda_D$. Representative values for λ_D are taken from *Garrett* [1981] and combined with altitude profiles of plasma densities in the plasmasphere [*Horwitz et al.*, 1990] and in the ionosphere [*Banks and Kockarts,* 1973] in order to calculate the electrostatic stress on the mantle surface shown in Figure 1. On the basis of the altitude profile of these electrostatic forces we agree with *Dessler* [1991] that there are no planet-wide sharp gradients of force at his nominally adopted breakup altitude of ~3000 km. The gradient occurs at altitudes ~1000 km. We use this latter, more realistic value for the breakup altitude.

Water at altitudes ~300 km injected during a rocket-borne experiment may have been marginally detected with the ultraviolet imager on Dynamics Explorer 1 [*Mendillo et al.,* 1990]. Loss of visibility of the cometary water vapor cloud at altitudes ~300 km is also consistent with the calculations by *Meier* [1987]. Thus the water vapor and clusters from the cometary core must be dispersed into a cloud with diameter ~50 to 100 km during the transit time from 1000 km to 300 km (see following section 2.2.2).

The electrostatic stresses on the comet as shown on Figure 1 are minimum values derived with the assumptions of a smooth exterior surface. for the mantle of the small comet. It is not unreasonable to assume that the heights and lateral dimensions of the surface topology exhibit irregularities on scales of ~1% of the diameter of the object, i.e., ~10 cm. When λ_D is large, for example, in the outer magnetosphere and solar wind, the electrostatic stresses can be expected to increase only by factors in the range of 10 at most relative to smooth-surface values [cf. *Harnwell,* 1949].

On the other hand, as the small comet enters the ionosphere at altitudes at ~1000 km the Debye sheath rapidly collapses in thickness. For example, the Debye length A, is only ~5 cm at 1000 km and protrusions from the mantle surface are likely to extend beyond the sheath. The calculation of the expected electric fields on these protrusions is not straightforward: extensive numerical modeling is required. In a conceptual sense we suggest that the outer boundary of the Debye sheath can be treated as a ground plane with respect to the ambient plasma and that the maximum electric fields on the charged protrusions are characterized by their radii for points and edges. For example, the electrostatic stresses for such radii of 10^{-2} and 10^{-3} cm are ~0.4 and 40 dyne/cm^2, respectively. These stresses are factors ~3 x 10^5 and 3 x 10^7 greater than those of a smooth sphere at an altitude of 1000 km. If such electrostatic forces are yielded by the collapse in Debye sheath thickness then rapid erosion of the mantle material could be expected with subsequent destruction of the integrity of the mantle and disruption of the cometary core. An appropriate analogy may be the action of sandpaper on the surface of a gas-filled balloon.

The above scenario for removal of the mantle material is only intended to provide an example of a mechanism to disrupt a small comet at altitudes of ~1000 km. However,

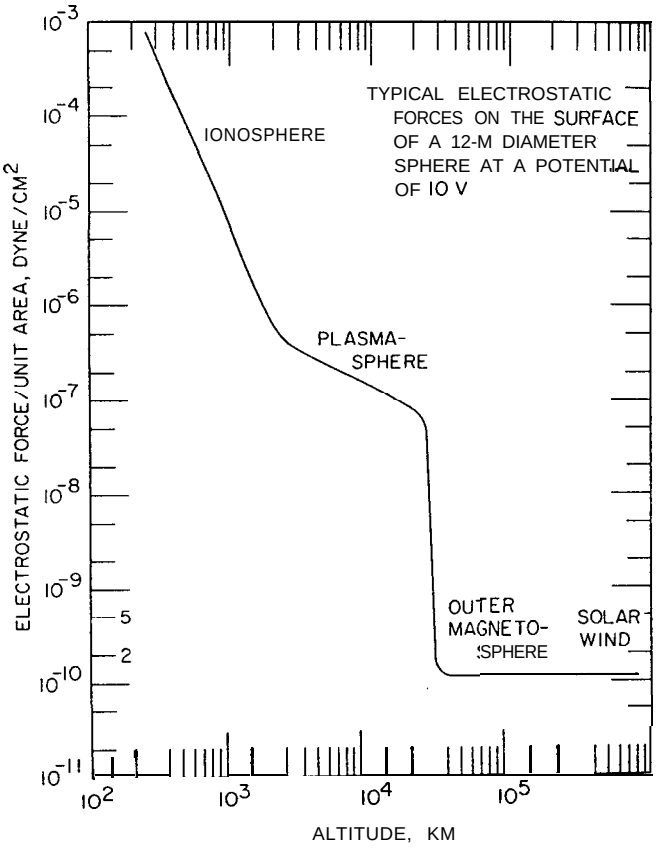

Figure 1. Typical electrostatic forces per unit area on the surface of a smooth sphere with radius 6 m and at a potential of 10 V as a function of altitude above the dayside surface of Earth. A steep gradient in these forces with decreasing altitude occurs at ~1000 km.

it is quite clear that a large increase in electrostatic stress with decreasing altitude occurs at altitudes ~1000 km (see Figure 1). In addition, at these same altitudes the severe decrease of the thickness of the Debye sheath to dimensions similar to, or smaller than, reasonable expectations for dimensions of surface protrusions of the mantle can greatly amplify these forces. Rapid electrostatic erosion appears to be a reasonable candidate mechanism for stripping the thin protective mantle from the water snow core of a small comet.

2.2. **Vaporization of ice Particles**

Dessler [1991] stresses that the lifetimes of ice particles in space are inconsistently long relative to the vaporization times required to produce a cometary water vapor cloud before impact with Earth's upper atmosphere. Indeed, we expect the water clusters produced during the disruption of the cometary core to have a comparable effective lifetime with respect to the time of flight from initial disruption until atmospheric entry, tens of seconds. We also note in the following section that (l*a*) derived by *Dessler* [1991] for ice particle lifetimes is inconsistent with experiments conducted in space.

2.2.1. **Apollo and space shuttle events.** We suggest the possibility that the effective lifetimes of the water clusters

within the cometary water cloud are sufficiently long such that a significant number of water clusters are present upon impact of the cometary water cloud with the upper atmosphere. Consider a 2×10^7-g water cloud as it radially expands after disruption. Assume that the composition of the cloud is 90% water clusters and 10% molecular water. For the following calculation the typical radius of a cluster is taken as 5×10^{-8} cm, or ~17 H_2O molecules. As the water cloud expands, the molecular water is rotationally cooled [*Delsemme,* 1982]. Thus the capture of the water molecule onto a water cluster during collision is probable. Collision frequencies in the expanding water cloud are consistent with this possibility. For a molecular speed of 500 m/s the collision frequencies of the water molecules with the water clusters are ~3 $\times 10^{-4}$, 0.3, and 5 s when the radius of an expanding, homogeneous cloud is 1, 10, and 25 km, respectively. Thus we expect that a significant fraction of the mass of the cometary water cloud can be weakly hydrogen bonded into dimers and clusters upon impact with the atmosphere. A quantitative evaluation depends upon the currently undetermined lifetime of such water clusters in space.

Dessler [1991] cites observations of liquid hydrogen and oxygen dumps from Apollo 14 and water dumps from the Space Shuttle as support for his conclusion that water ice particles are long-lived in space. The most appropriate observations, not mentioned by *Dessler* [1991], are available from an experiment conducted on board Space Shuttle Discovery during orbit 49 of mission STS-29, March 16, 1989 [*Pike et al.*, 1990]. The lifetimes of ice particles with typical radii of 0.2 μ, which are formed by forced water ejection from a conical nozzle with a small aperture, are determined to be ≳ 250 s. Application of (l*a*) derived by *Dessler* [1991] predicts that this lifetime is 9 s, grossly inconsistent with the observational results. The error in his equation is possibly related in part to the assumed value of ε, the absorptivity of the ice particle.

In addition, the equation for the lifetime of an ice crystal in space as given by *Dessler* [1991] in his Appendix A is not generally valid. To first order, the lifetime is proportional to the energy absorbed by the ice particle. For the water clusters with radii ~ 10^{-7} cm of interest to the present work, the absorption of energy is proportional to the volume of the particle rather than the area of the particle as assumed by *Dessler* [1991]. Absorption cross sections for Rayleigh scattering by isotropic Rayleigh spheres are given by *van de Hulst* [1957]. We are in qualitative agreement with *Dessler* [1991] that small ice crystals in space are relatively long-lived, i.e., our assumption that lifetimes for the molecular water clusters are similar or greater than their flight times into the upper atmosphere.

2.2.2. **Application to small comets.** Consider the nucleus of water snow at 1000 km, that is stripped of its protective mantle. The nucleus disintegrates, perhaps as a result of tidal force and/or gas pressure from rapid sublimation of the water snow. The travel time from this altitude to loss of visibility of the object at ~300 km [*Mendillo et al.,* 1990] is ~50 to 70 s for a speed of ~20 km/s and angles of incidenc ~30° to 45° into the upper atmosphere. Is there sufficient time for a cloud of water molecules and clusters to expand to radial dimensions in the range of 25 km before impact?

The early stage of expansion is the most critical. Without speculation upon the details of the process, insight can be obtained by considerations of the energies available and required for the initial expansion. For example, assume that the cloud of water vapor and molecular clusters reaches a radius of ~2 km at a time 10 s after loss of the mantle. The average radius of this sphericai cloud is assumed to be ~1 km for the 10-s interval and the entire cloud mass, 2×10^7 g, is assumed to be moving with a radial speed of ~200 m/s. Because the initial speed of the sublimated water molecule is ~860 m/s [*Delsemme,* 1982; *Lammerzahl et al.,* 1987] only ~5% of the cloud mass need be sublimated to impart the radial velocity through energy equipartition by collisions between water molecules and water clusters. The sublimation energy for the water clusters is unknown, but we will assume a conservative value, 7.9×10^{-13} erg/H_2O molecule for water snow [*Delsemme and Miller,* 1971]. The total energy required for sublimation is then 3×10^{16} erg. The total kinetic energy of the cometary cloud is only ~4×10^{15} erg. The available insolation during this initial 10-s period is ~4×10^{17} ergs; i.e., only ~8% of the available solar energy is necessary to produce this initial stage of the cometary water cloud. For comparison, *Delsemme* [1982] estimates that ~17% of the incident solar radiation produces vaporization for bare cometary water snow at 1 AU. Thus the formation of this initial, expanding cloud is reasonable from considerations of the total available energy.

Sublimation of the cometary water clusters proceeds by insolation until impact into the upper atmosphere. The radial expansion speed increases as the ratio of water cluster mass/vapor mass decreases. Anticipated radial speeds of expansion are then in the range of ~400 to 860 m/s before this impact. If the average speed is 500 m/s, then the cloud radius is ~25 km. For the parameters we have chosen above, approximately 25% of the cometary mass is sublimated by the time it reaches an altitude of ~300 km, and the radial expansion speed is 430 m/s.

For a cloud radial expansion speed of 500 m/s the expansion in radial dimensions of the cloud from ~25 to 35 km occurs in ~20 s. These radial dimensions are consistent with observations with the Dynamics Explorer 1 imager, i.e., with the time interval required for the detection of atmospheric holes in several adjacent scan lines [*Frank et al.,* 1986*g; Sigwarth,* 1988].

2.3 Small-Comet Event Rate

A comprehensive description of the three spin-scan imaging photometers on board Dynamics Explorer 1 is given by *Frank et al.* [1981]. The fields of view and sampling times used for the acquisition of the pixel arrays (images) are fully defined in the above reference.

The usual acquisition time for an image from the ultraviolet photometer is 720 s. At apogee, and when a large

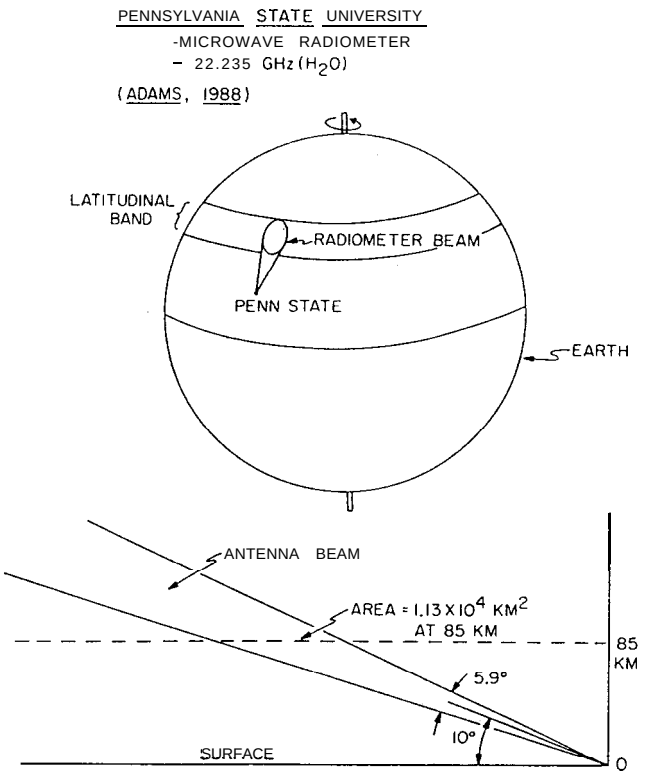

Figure 2. Viewing geometry for the Penn State microwave radiometer that is used to monitor water vapor in the mesosphere and thermosphere [after *Adams,* 1988].

fraction of the sunlit hemisphere is viewed, typically 3 to 7 atmospheric holes are detected in a single image. An atmospheric hole is defined by *Frank et al.* [1986*a*] as a localized decrease in the dayglow intensities corresponding to a $\geqslant 4.30$ (or $\gtrsim 50\%$) decrease in photometer responses. Most often these decreases occur in a single pixel. The instantaneous, conical field of view of the photometer is 0.32°. The corresponding field of view of a single pixel for which the sample time within this field of view exceeds one half of the sampling time, i.e., > 1.7 ms, is 0.29°. At an altitude range of 15,000 to 23,000 km from which most of the images are acquired, this latter solid angle corresponds to a range of diameters of ~76 to 117 at Earth's upper atmosphere. For an object that totally absorbs the dayglow, the corresponding range of object diameters is ~53 to 83 km for a 50% decrease in pixel responses. A representative diameter at the lower bounds of this range, ~ 50 km, is selected by *Frank et al.* [1986*b*] in the interpretation of the transient dayglow decreases in terms of cometary water clouds.

Given the number of atmospheric holes in the images, a lifetime for the atmospheric holes is required to determine the global rate. This lifetime is estimated by *Frank et al.* 1986*a*] from higher time resolution images of atmospheric holes. The duration of the intensity decreases at > 4.3σ is ~1 min [see *Frank et al.,* 1986*a,* Figure 4]. From this information the global rate is estimated as ~20 events/min.

The rate of small-comet impacts into Earth's upper atmosphere as derived from the observations of atmospheric holes with Dynamics Explorer 1 is similar, within factors of 2 to 3, to the rates determined from direct telescopic detection of small comets (see section 5.2.1) and from the transient bursts of microwave radiation from hot water vapor in the upper atmosphere (see section 3). Because of the very limited number of dayglow images from the Viking satellite and the correspondingly sparse number of atmospheric holes detected in these images, only an order-of-magnitude estimate of the occurrence rate is available (see section 5.1**).** This occurrence rate is consistent with the Dynamics Explorer 1 observations of atmospheric holes.

3. IONOSPHERIC AND ATMOSPHERIC EFFECTS

In this section, *Dessler* [1991] identifies two topics: (1) the search for atmospheric water bursts associated with the infall of small comets with the Pennsylvania State University (Penn State) microwave radiometer and (2) orbital mechanics for small comets. The first topic is discussed here. The second topic is more appropriately examined in section 4.2. However, it is noted here that *Dessler* [1991] has miscited *Frank and Craven* [1988] as to the source of the small comets. *Frank and Craven* [1988] identify the source region as the Oort inner disk, not the Oort cloud as given by *Dessler* [1991]. The proper identification of the source region is important because of the distribution of orbits, i.e., low-inclination, prograge orbits in the inner disk and the full range of orbital inclinations in the Oort cloud.

The Penn State microwave radiometer is routinely used to monitor water vapor in the mesosphere and the thermosphere [*Bevilacqua et al.,* 1983; *Tsou,* 1986]. Observations of the

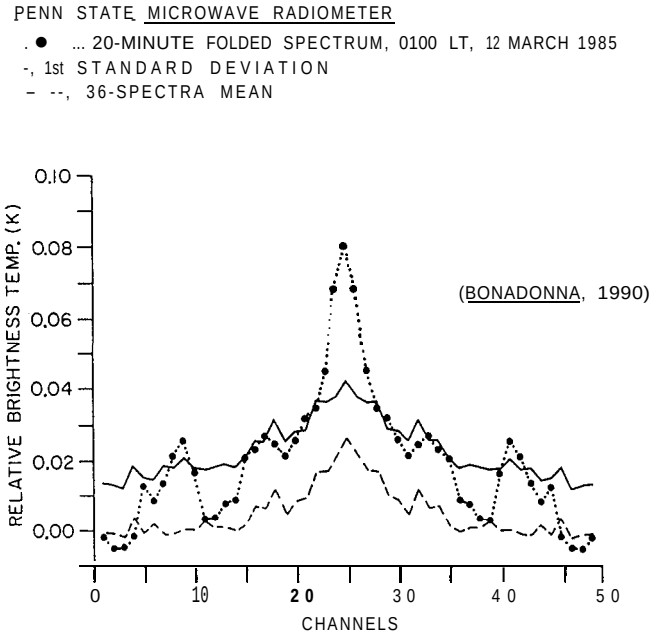

Figure 3. Example of an impulsive increase in the water microwave emissions at 22.235 GHz as observed at 0100 LT on March 12, 1985. Relative brightness temperature as a function of frequency (channel) is shown. Line center is located at channel 25, and the spectral resolution is 50 kHz [after *Bonadonna,* 1990].

spectrum of the Doppler- and pressure-broadened water emission line at 22.235 GHz are inverted to obtain the water vapor densities as a function of altitude. The viewing geometry for the radiometer is shown in Figure 2. The antenna receiving beam is steerable and is usually pointed toward the northeast with elevation angles ranging from 10° to 30°.

Observations of the water emission line are normally averaged over periods of typically 12 hours to provide accurate altitude profiles of water densities. These densities fluctuate slowly on such time scales. On the other hand, the impact of a small comet into the atmosphere should produce a transient increase, or burst, as its water vapor transits the field of view of the microwave radiometer. In order to search for such bursts the microwave spectra are examined at 20-min resolution [*Adams et al.,* 1987; *Adams,* 1988; *Bonadonna,* 1990; *Bonadonna et al.,* 1990]. An example of an atmospheric water burst as detected with the microwave radiometer is shown in Figure 3 [*Bonadonna,* 1990]. Relative brightness temperatures as a function of frequency (1 channel = 50 kHz) are displayed for the water burst, the mean background from the 36 20-min spectra taken closest in time for the event, and the first standard deviation for these background spectra. Relative brightness temperatures are not scaled to the system gain, and actual values are greater by factors of 2 to 4 [*Bonadonna,* 1990]. The probability that the spectral signature centered at channel 25 in Figure 3 is produced by random noise is $\sim 2 \times 10^{-7}$ and is one of the lower values for the water bursts detected with the microwave radiometer.

Bonadonna [1990] examines 22,832 20-min microwave spectra for water bursts. These data are taken during the period December 4, 1984 through November 30, 1988. The number of statistically significant events is 111. The probabilities that the individual events are produced by random noise range from $\sim 2 \times 10^{-28}$ to 1.2×10^{-4}. Even if all the events are at the selection threshold probability of 1.25×10^{-4}, fewer than three events are expected to be due to random noise for the entire data set. The detection of these water bursts is based upon a rigorous statistical analysis by *Bonudonna* [1990].

The rate of detection of water bursts with the Pennsylvania State University microwave radiometer is one event every 2.9 days. The corresponding rate that is anticipated from observations of atmospheric holes with Dynamics Explorer 1 is one event every 1.8 days. *Adams* [1988] estimates that the contents of the water bursts observed with the microwave radiometer are in the range $\sim 10^{29}$ to 10^{34} H_2O molecules, or $\sim 3 \times 10^{6}$ to 3×10^{11} g. Thus the results from the microwave measurements of the bursts of thermal water emissions in the upper atmosphere are in general agreement with predictions obtained from observations of transient decreases in ultraviolet dayglow emissions, or atmospheric holes, with Dynamics Explorer 1.

3.1. **Ionospheric Effects**

Because of the complexity of the interaction of this water cloud with the ionosphere, it is difficult to predict whether or not there will be enhancements or reductions in plasma densities and plasma heating [*Hanson,* 1986]. Of primary interest here is the electrodynamical and collisional interaction of the supersonic cometary material with the neutral gases and plasmas in the ionosphere, for example, charge exchange, in contrast to modification of ionospheric chemistry by the direct deposition of water with rocket-borne experiments (cf. section 3.1.1). In any case, the search for such signatures is limited to subauroral magnetic latitudes in the dayside ionosphere in order to avoid the plasma fluctuations that exist because of other physical processes in the auroral and polar ionospheres. *Dessler* [1991] cites the results of *Hanson*'s [1986] search for spatial variations with scale sizes 50-100 km in the low-latitude *F* region ionosphere with in situ measurements with three spacecraft: no detectable variations are observed. Accordingly, *Frank et al.* [1986*f*] propose that the cometary water cloud and its ionization are transported across the magnetic field in the ionosphere by means of polarization electric fields that produce a $\mathbf{E} \times \mathbf{B}$ drift velocity in the same direction and with the same speed as the cometary water vapor cloud [*Schmidt,* 1960; *Baker and Hammel,* 1965; *Barney and Sprott,* 1969]. If this were the primary interaction, then the principal signature of the passage of the cometary water vapor cloud might be expected to be a turbulent wake. *Frank et al.* [1986*f*] report several examples of turbulence with scale sizes ~100 km in the ionospheric densities observed with Hanson's instrument on Dynamics Explorer 2. *Dessler* [*1991*] cites Hanson in private communication as attributing these events to instrumental effects and a spacecraft-plasma interaction.

Dessler [1991] also states that the electric field $-\mathbf{V} \times \mathbf{B}$ used above by *Frank et al.* [1986*f*] for cometary plasma transport through the ionosphere is zero when the comet is moving parallel to **B.** Thus he implies that a significant number of these cometary water clouds are unaffected by the proposed transport mechanism. Dessler fails to recognize the fact that the magnetic fields in the low-latitude ionosphere are grossly oriented perpendicularly to the ecliptic plane. Thus, with the proposed cometary orbital motion near the ecliptic plane and hence more or less perpendicular to **B,** Dessler's criticism is inapplicable.

We are greatly influenced in our past ionospheric investigations by *Hanson*'s [1986] examples of very smooth density profiles in the low-latitude dayside ionosphere and the accompanying descriptive text. The threshold for his search is set at deviations greater than 20% although the instrumentation is quite capable of revealing much lesser fluctuations. *Dessler* [1991] cites these results. Recently, L. H. Brace (private communication, 1991) identifies several examples of localized regions of lesser ionospheric densities as observed at low latitudes in the sunlit ionosphere with a Langmuir probe on Dynamics Explorer 2. One such decrease is shown at about 2053 UT on September 21, 1982, in Figure 4. The observations are taken in the late-morning hours in order to avoid *F* region "fossil" bubbles, a requirement also imposed by *Hanson* [1986] in his survey for ionospheric fluctuations. The decrease in ionospheric densities is ~20%,

with a full spatial width of ~130 km. An increase of electron temperature of ~300 K is detected coincident with the decrease in plasma density. R. A. Hellis (private communication, 1991) confirms that the density decrease is also detected with the retarding potential analyzer that is used by W. B. Hanson on the same spacecraft. It is not presently possible for us to determine whether this density decrease is due to the passage of a cometary water cloud through the ionosphere (the scale size is appropriate) or whether the decrease is due to an unrelated ionospheric phenomena. However, the impression given by *Dessler* [1991] that significant density fluctuations of the appropriate scale size in the low-latitude dayside ionosphere do not exist is clearly contradicted by the observations.

The rate of detection of plasma density decreases as a result of passages of cometary water clouds is dependent upon the time constant for filling the void. *Hanson* [1986] estimates a filling time of ~10 min due principally to photochemical processes by using the model by *Bailey and Heelis* [1980]. However, the spatial gradients in the density depression shown in Figure 4 are large and, if due to passage of a water cloud, the total loss of plasma in the magnetic flux tube is only several percent. Plasma instabilities associated with the density gradient might provide redistribution of the plasma within the flux tube on much lesser time scales. If plasma transport into the localized void is characterized by the O^+ thermal speeds, ~1 km/s, then the refilling times would be of the order of tens of seconds and the corresponding detection rate would be only about one event for every 10 hours in the low-latitude dayside ionosphere.

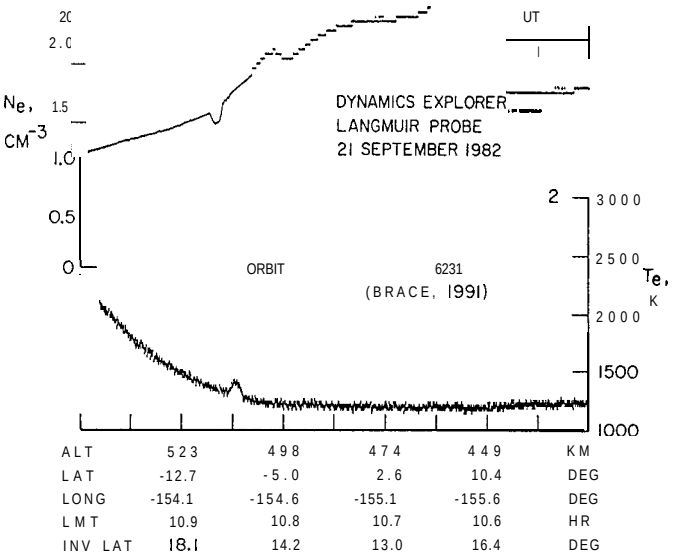

Figure 4. Example of a decrease of plasma densities at low magnetic latitudes in the ionospheric F region at ~2053 UT September 21, 1982 (courtesy of L. H. Brace, 1991). Is this decrease due to the passage of a cometary water cloud or due to an unrelated ionospheric phenomenon? An increase in electron temperature T_e also occurs. Spacecraft atltitude (ALT), geographic latitude (LAT) and longitude (LONG), local magnetic time (LMT), and invariant latitude (INV LAT) are given along the abscissa.

3.1.1. **Water vapor deposition in the ionosphere.** *Dessler* [1991] claims that a significant fraction of the cometary water clouds, those with grazing angles of incidence into the atmosphere, are stopped and hence deposit their entire vaporous contents at altitudes ~125 to 300 km. Clearly, such deposition of water would exceed the observational limits in this region of the thermosphere by orders of magnitude. However, the depth of penetration into the atmosphere for a supersonic ball of water vapor presents a formidable computational task.

The model employed by *Dessler* [1991] assumes a straight-line trajectory into the upper atmosphere and continuous expansion of the water vapor at its characteristic thermal speed. We intend here only to demonstrate the frailty of his results because a credible numerical simulation of this impact is not available. We consider two major effects neglected by Dessler: gravity and ram pressures.

First of all the presence of a gravitational field is accounted for. We use our usual simplification of a homogeneous cylinder of water vapor with circular cross-sectional area 2.0 $\times 10^{13}$ cm^2 (r = 25 km). The total mass is 2 $\times 10^7$ g, or 7 $\times 10^{29}$ H_2O molecules. The initial speed is 20 km/s and three angles of incidence $\theta = 0°, 45°$, and 90^0 (grazing incidence) are selected as examples. Atmospheric gases impacting the water cloud along the water cloud trajectory are assumed to be accumulated into the gas cloud and linear momentum is conserved [*Frank et al.*, 1986*c*]. *Jacchia*'s [1977] tables for atmospheric mass densities corresponding to an exospheric temperature 1000 K are used. The results are shown in Table 1. The coordinate X is taken along Earth's surface, and Y is altitude. Inspection of Table 1 finds $V = (V_x^2 + V_y^2)^{1/2} \gtrsim 0.5$ km/s at an altitude of 115 km for all angles of incidence. The corresponding local sonic Mach number is ~1. This result is to be contrasted with *Dessler*'s [1991] conclusion that the cometary water clouds are stopped at considerably greater altitudes.

In order to further increase the altitude limits for penetration of the water vapor clouds, *Dessler* [1991] assumes that the cloud continues to expand at water molecular speeds, ~500 m/s, as in vacuo. This expansion increases the intercepted atmospheric mass and thusly increases the deceleration at a given altitude. However, the atmospheric ram forces are large relative to the gas pressures within the incoming water vapor cloud. If we take a benchmark water vapor temperature of 1000 K and water vapor number density 10^{10}/cm^3, then the internal cloud pressure is 1.4 $\times 10^{-3}$ dyne/cm^2. The ram pressures are calculated directly from the speeds shown in Table 1. For examples, at altitudes 400, 200, 115, and 80 km and $\theta = 0^o$ the ram pressures are 8 $\times 10^{-3}$, 2.8, 4.2 $\times 10^{-1}$, and 9 dyne/cm^2, respectively. Such ram pressures can be expected to compress the water vapor cloud, decrease its cross-sectional area, and increase the speeds at lower altitudes relative to those given in Table 1.

The complexity of accurately determining the characteristics of the cometary water impact rapidly becomes apparent: now include compression and heating of the water vapor,

TABLE 1. Atmospheric Trajectory Parameters for Cometary Water Cloud Impacts Using a Simple Gas-Piston Model Plus Gravity

Elapsed Time, s	*X, km*	*Y, km*	V_x, *km/s*	V_y, *km/s*	*M, g*
		$\theta = 0°$			
0	0	400	0	- 20.0	2.0×10^7
14	0	200	0	-6.7	6.0×10^7
54	0	115	0	-0.52	1.0×10^9
179	0	80	0	-0.26	1.7×10^{11}
		θ = 45"			
0	0	400	14.1	- 14.1	2.0×10^7
21	200	200	3.68	-3.8	7.6×10^7
84	270	115	0.22	-0.42	1.3×10^9
210	280	80	0.0	-0.25	1.8×10^{11}
		$\theta = 90°$			
0	0	400	20.0	0	2.0×10^7
276	2640	200	2.02	-0.88	2.0×10^8
383	2750	115	0.27	-0.45	1.5×10^9
504	2760	80	0.0	-0.25	1.8×10^{11}

ablation of the vapor, properties of the postshock gas from the Rankine-Hugoniot relationships, cooling from infrared radiation, etc. However, inclusion of zero-order effects into our rudimentary model, namely gravity and ram forces neglected by *Dessler* [1991], clearly demonstrates that the water vapor cloud will pass into the mesosphere with substantial speeds regardless of its angle of atmospheric impact.

The precise altitude that the cometary water cloud and its accreted atmospheric mass will come to rest in the mesosphere is uncertain without detailed numerical simulation. These gases are slowed to speeds comparable to those of the zonal winds, tens of meters per second, and subsequently dispersed. The final depth of penetration depends importantly on the cross-sectional area of the piston. As stressed by *Dessler* [1991], the calculation by *Banks* [1989] demonstrates that cooling due to infrared radiation should be rapid. Such cooling acts to reduce the gas volume and increase the depth of penetration into the mesosphere. We have previously estimated a final depth of penetration from very oversimplified estimates as ~ 55 km [*Frank et al.,* 1986*c*].

Mendillo et al. [1990] report the pyrotechnic release of ~100 kg of water vapor from a rocket payload at an altitude of ~300 km. The rocket speed is ~1.2 km/s generally downward toward Earth's surface. The deposition of this water vapor in the ionosphere produces a large region of decreased ionospheric plasma densities. On the other hand, the cometary water cloud is traversing the ionosphere at supersonic speeds, 15 to 20 km/s, and the amount of water deposited at these altitudes is dependent upon the details of entrainment in the wake. If the cometary water cloud is stopped at ~55 km altitude and if the entrainment of cometary water vapor proceeds at a constant mixing ratio, then the amounts of water deposited in the upper atmosphere at altitudes ≥300 km and ≥200 km are ~4 and 40 g, respectively. If this is a valid approximation for the amount of entrained water, then the ionospheric plasma depletions due to modification of ionospheric chemistry are lesser by orders of magnitude than those for the depositions of water with rockets.

The depth of atmospheric penetration is also important because deposition of the cometary water below the homopause, i.e., the altitude (~100 km) above which molecular diffusion dominates over transport by vertical atmospheric motions for lower altitudes, will circulate the water vapor through the tropopause by atmospheric advection. Cold temperatures at the tropopause will precipitate the cometary water vapor into the troposphere and dry the atmospheric gases rising above the tropopause [cf. *Brasseur and Solomon,* 1984]. Deposition of the cometary water vapor above the homopause would yield observationally unacceptable H_2O, OH, and H densities in the thermosphere [*Donahue,* 1986].

3.2. Aeronomic Effects

Reid and Solomon [1986] and *Solomon et al.* [1982] conclude that the observations of the altitude profiles of water vapor in the upper mesosphere and lower thermosphere are suggestive of a source of water from above Earth's atmosphere. Further, *Reid and Solomon* [1986] use a one-dimensional diffusion model to demonstrate that the cometary water influx, ~3 x 10^{11} H_2O molecules $cm^{-2}s^{-1}$, as proposed by *Frank et al.* [1986*b*] is too large to be consistent with the observed water densities. Their diffusion model assumed that the water density at the upper boundary altitude of 116 km is fixed at 3.5 ppmv and that the cometary water is diffusing downward from this upper boundary altitude. *Frank and Craven* [1988] note that the momentum of the cometary water vapor cloud can be expected to carry it to significantly lower altitudes, ~ 50 to 60 km, relative to the 116-km altitude assumed by *Reid and Solomon* [1986]. Thus the diffusion equation must contain a source term. In addition, *Garcia and Solomon* [1983] show that a one-dimen-

sional transport model for water in the middle atmosphere is inadequate. In fact, *Bevilacqua et al.* [1990] conclude that diffusion is of secondary importance relative to advection in determining the water vapor distribution in the mesosphere. The inclusion of (1) an appropriate water source term and (2) mesospheric advection lessen considerably the restrictions on an interplanetary source of water vapor relative to that given by the one-dimensional diffusion model of *Reid and Solomon* [1986]. Their upper limit for an influx of extraterrestrial water is $\sim 10^{10}$ H_2O molecules $cm^{-2} s^{-1}$. This upper limit can be expected to be considerably larger if the appropriate source term and atmospheric circulation are included. We note that the influx of cometary water vapor is currently estimated to be $\sim 6 \times 10^{10}$ H_2O molecule $cm^{-2} s^{-1}$ on the basis of the telescopic detections of the small comets (see section 5.2.1).

3.2.1. **Atomic hydrogen.** In his criticism of the proposed influx of small comets into Earth's upper atmosphere by *Frank et al.* [1986*b*], *Donahue* [1986] correctly states that the water densities in the mesosphere and thermosphere would be unacceptably large by orders of magnitude if (1) the cometary water is deposited above 90 km and (2) a one-dimensional model for transport only by molecular and eddy diffusion [*Hunten and Donahue,* 1976] is assumed. Effects of such high densities include (1) geocoronal hydrogen densities that are orders magnitude larger than observed values, (2) a global ice cloud at the mesopause, and (3) destruction of virtually all mesospheric ozone. *Frank et al.* [1986*c*] point out that penetration of the cometary water clouds to altitudes ~55-60 km (see section 3.1.1) and atmospheric advection (see section 3.2) can allow the proposed water influx to be accommodated by the observed magnitudes of water densities in the middle atmosphere with reasonable values for the vertical transport speeds. In this case the three effects noted above by *Donahue* [1986] do not occur.

3.2.2. **Heating and IR radiation.** The difficulties in quantitative computation of the properties of the impact gases at altitudes where the energy loss is greatest are already noted in section 3 .1 . 1. Only detailed numerical modeling can yield reliable estimates of such parameters as bulk speed versus altitude, radiative losses, ionization states, etc. *Banks* [1989] also notes these difficulties and limits his calculations of the infrared emissions from the incoming water clouds to altitudes $\geq$ 200 km. For these higher altitudes, Banks computes the radiance and total emitted power from the water cloud for the bands at 2.66, 2.74, and 6.27 μ due to direct excitation by solar and terrestrial radiation and by collision of cometary water molecules with atmospheric atomic oxygen. The main thrust of Bank's paper is to show that current infrared instrumentation is capable of detecting these water clouds if such equipment is space-borne.

4. SOLAR-SYSTEM EFFECTS

Dessler [1991] concludes that there are inconsistencies of a large population of small comets in the inner solar system with (1) lunar impacts and (2) interplanetary water sources due to vaporization from small comets, lunar impacts, and near-misses with Earth. Our responses follow. A possible mode of cometary water disposition at Mars is given by *Frank et al.* [1986*c*].

4.1. lunar Impacts

Dessler [1991] asserts that total energy and momentum of an impactor on the Moon are the primary parameters that determine the crater size and the amplitude and frequency spectrum of the seismic waves. Thus the crater sizes and seismic waves should be similar for the impacts of a stony meteoroid and of a loosely bound snowball if their total energies and momenta are the same. Similar arguments are used by *Davis* [1986], *Baldwin* [1987], and *Nakamura et al.* [1986], although the latter authors note that the density of the impactor may be important.

It is well established that the scaling laws for crater sizes and the seismic spectra for dense ($\gtrsim 1$ g/cm³) impactors depend upon the energy and momentum of the impactor [*Holsapple and Schmidt,* 1982, and references therein]. If these scaling laws for dense impactors also apply to impactors with considerably lesser densities, for example, 0.01 to 0.1 g/cm³, then the observations with the Apollo seismic stations most certainly exclude the existence of the small comets.

There is valid reason to question extrapolation of cratering sizes and seismic spectra to impactors with very low densities. Although there are no published experimental data for such low-density, porous impactors, *O'Keefe and Ahrens* [1982] report numerical simulations of the impacts of water ice and water snow onto gabbroic anorthosite and silicate targets. Their results for impactors with initial speed V = 15 km/s and mass densities 1, 0.1, and 0.01 g/cm³ are shown in Figure 5. The total mass of each impactor is 2×10^7 g and the corresponding impactor diameters (d) are shown in the figure. The times after impact are $t = 1.50$, 1.95, and 5.10 τ for impactors with densities 1, 0.1, and 0.01 g/cm³, respectively, where $\tau \equiv d/V$. It is important for the reader to recognize that the total energies and momenta of the three impactors are equal, but the qualitative characters of the impacts differ greatly. These results contradict the assertion by *Dessler* [1991] that scaling of such impacts depends on total energy and momentum, regardless of the impactor's density. The impact of the projectile with density 1 g/cm³ (water ice) is similar to that of a meteoroid with higher densities, for example, deep cratering of the target, a large fraction of impactor energy transferred to the target, and high particle speeds associated with a shock wave in the target. The scale for the particle motions is given at the upper left of each of the three diagrams. As the density of the impactor decreases, the particle motions, and the seismic amplitude, in the target rapidly decrease and the crater depths decrease. Note that the diameter of the crater is considerably larger than the diameter of the 1-g/cm³ impactor, but at lower densities the crater and impactor sizes are similar. For the low-density impactors, most of the impact energy is carried away

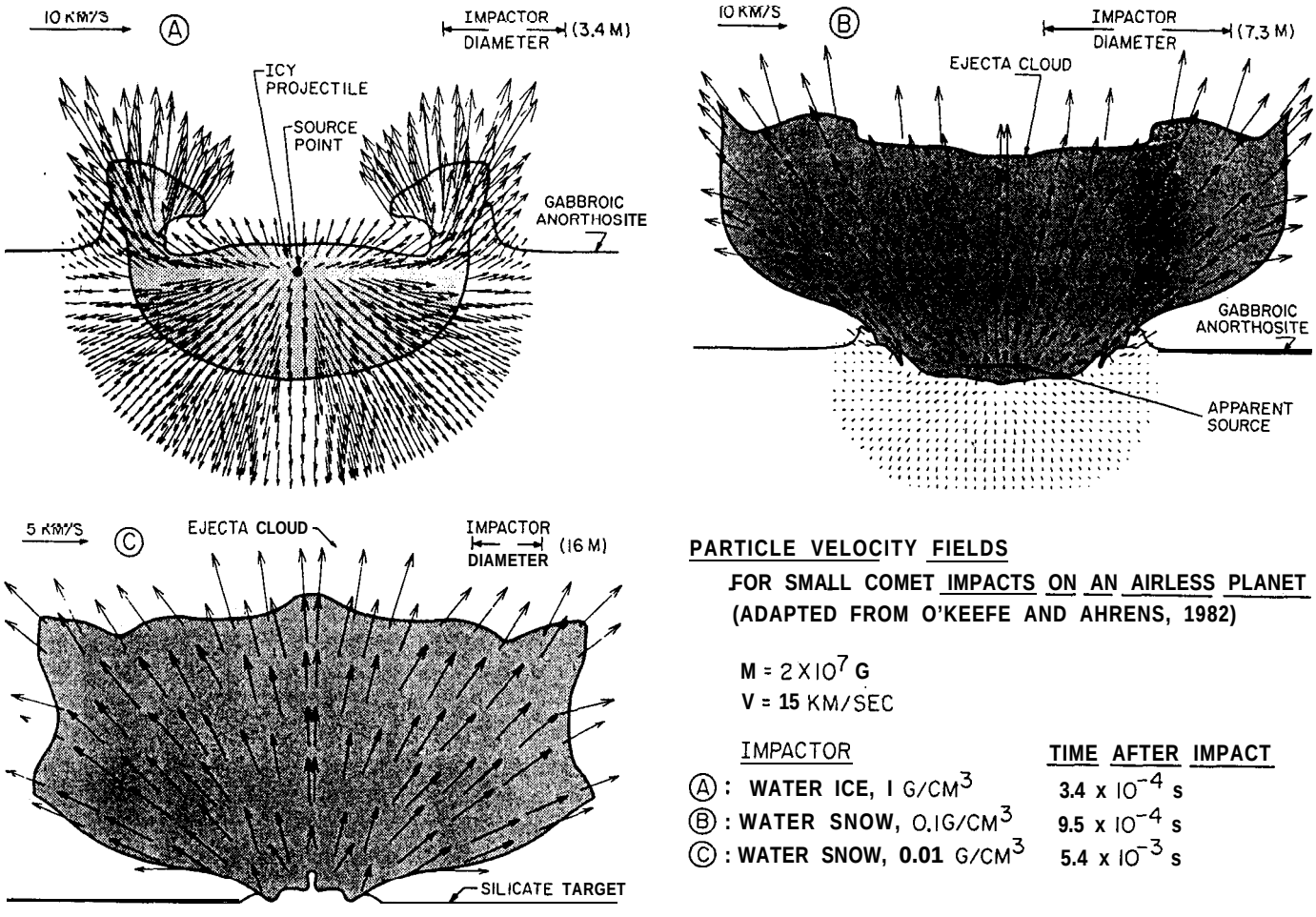

Figure 5. Numerical simulations of the impacts of 2 X 10^7 g small comets on gabbroic anorthosite and silicate targets at speeds of 15 km/s (adapted from *O'Keefe and Ahrens* [1982]). The mass densities are (a) 1 g/cm³, (b) 0.1 g/cm³, and (c) 0.01 g/cm³. The total energy and momentum are the same for all three impactors.

by the postimpact cometary gases. The frequency spectrum of the small amount of seismic energy that does propagate into the target is not investigated with this numerical simulation.

These results concerning low-density impactors are similar to the conclusions on less rigorous grounds by *Frank et al.* [1986*h*]. The presence of a layer of soil over the lunar surface is not considered and may be important in further cushioning the impact of a low-density projectile and determining the propagation of seismic waves from the impact site. The average flux of small comets impacting the lunar surface is $\sim 1.2 \times 10^{-19}$ cm^{-2} s^{-1} (see section 4.1.1), or ~4 X 10^5 events/yr. The observed rate of meteoroid impact events at an Apollo seismometer is ~ 200 events/yr [*Latham et al,* 1973]. Given the inefficient energy transfer from low-density impactors to the lunar surface [*O'Keefe and Ahrens,* 1982] and the threshold amplitudes of $\sim 10^{-8}, 10^{-6}$, and 5 x 10^{-2} cm for wave periods of 0.1,0.05, and 0.01 s, respectively, for the Apollo seismometers [*Lathum et al,* 1973], it is quite possible that only a very small fraction of the small-comet impacts are seismically detected. Further research on seismic coupling of low-density impactors is required before this issue can be resolved.

Dessler [1991] asserts that impacts of the S-IVB stages of the Apollo Saturn V launch vehicles onto the lunar surface mimic the impacts of small comets. Large craters and seismic wave amplitudes are associated with the impacts of the S-IVB stages. The impact speed is ~2.5 km/s. *Dessler* [1991] states that the mass density of the S-IVB stage is ~0.025 g/cm³ because it is hollow. But consideration of the fact that metal sides and bulk heads of the S-IVB stages, with mass densities of approximately several g/cm³, are providing the impact dynamic pressure finds that the characteristics of the impact should be more similar to those for a stony or iron meteoroid (see, for example, diagram A in Figure 5). That is, the S-IVB stage is not a low-density, porous (homogeneous) impactor [cf. *Zel'dovich and Raizer,* 1967].

Frank et al. [1986*h*] suggest that a brief visible light flash from the expanding postshock cometary gases may be detectable with a suitably equipped ground-based telescope. The detection of occasional light flashes on the Moon is reported in the literature. For examples, *Latham et al.* [1972] note that the pilot of an Apollo command module observed a bright flash on the surface of the Moon at large distances from the seismometers which detected no correlated seismic waves, and *Kolovos et al.* [1988] discuss the appearance of

another bright flash of short duration in ground-based telescopic photographs. This latter paper provides further references for such lunar transient phenomena. *Mutel et al.* [1991] estimate that the apparent visual magnitude of the light flash is ~ - 5^m at ~40 ms after impact and $\lesssim 0^m$ for a time period of ~100 ms after impact. They discuss the design of a modestly sized telescope with a CCD camera to obtain ~1-2 x 10^6 images of the darkside of the Moon with ~100-ms resolution. One half of the images are to be taken at first-quarter Moon (null experiment), the other half at third-quarter Moon. Approximately 50 light flashes are expected in the latter image set. Such telescope observations may resolve the controversy concerning the nature of the impact of a small, low-density comet onto the lunar surface.

4.1.1. **Small-comet lunar atmosphere.** *Frank et al.* [1986*h*] note that the expanding cloud of water vapor from small-comet impacts on the lunar surface should produce a hydrogen coma similar to that of comet P/Halley. As viewed at large distances from the Moon, greater than or equal to several hundred R_E, *Frank et al.* [1986*h*] estimate that the maximum Lyman α brightness of the Moon's coma is ~80 R, an estimate based upon a model for comet P/Halley [*Meier and Keller,* 1985]. The lunar coma is characterized by a large spatial scale. When viewed from large distances the brightness decreases to 20% of its maximum value at lunar radial distances of ~150 R_s; i.e., Earth is embedded in the Moon's tenuous hydrogen atmosphere.

The brightness of the lunar coma depends upon the rate of small-comet impacts and the typical small-comet mass. As pointed out by *Sorer* [1987] and later by *Morgan and Shemansky* [1991], the conversion of comet fluxes at Earth's upper atmosphere into corresponding interplanetary fluxes by *Frank et al.* [1986*b*, 1987*a*] is in error. The average interplanetary fluxes are ~1.2 x 10^{-19} cm^{-2} s^{-1}, a factor of ~3.3 larger than the originally published values. The corrected impact rate for the Moon is then ~0.7 impacts/min. With this impact rate and the best estimate for average small-comet masses, ~2 x 10^7 g (see section 5.2.1) the above estimate of the maximum Lyman α intensities for the Moon's coma becomes ~50 R. Perhaps such intensities can be detected against the significantly brighter background from interstellar hydrogen if viewed from a favorable aspect. The Galileo ultraviolet spectrometer [*Hord,* 1992] offers the possibility of such detection during the spacecraft's Earth flybys.

Morgan and Shemansky [1991] compute line-of-sight intensities for OH 308.5-nm and 0 I 130.4-nm resonant emissions as a function of the viewing impact parameter. For modeling the spatial distributions of the OH and 0 I these authors assume that the entire contents of the small comets leave the lunar surface with a postimpact speed of 4 km/s. Three scenarios are examined: the postshock gas is (1) H_2O, (2) OH + H, or (3) 0 + H + H [*Morgan and Shemansky,* 1991, Table B2]. For an impact parameter of 1 R_M (lunar radius) the brightnesses for OH are 0.52 and 42.9 kR for (1) and (2) above, respectively. The corresponding brightnesses for 0 I are 1.07, 17.8, and 691 R for (1), (2), and (3) above, respectively. These intensities should be reduced by a factor of ~5 because of the current best estimate of cometary mass (see section 5.2.1).

The dissociative state of the immediate postshock water is unknown. Clearly, the intensities are larger with higher levels of dissociation immediately following impact relative to the intensities from the constituents of outflowing water that is photodissociated by solar radiation over much larger spatial scales. *Morgan and Shemansky* [1991] use qualitative arguments in favor of a highly dissociated state of postshock water, but there are no conclusive arguments that preclude molecular postshock water as assumed by *Frank et al.* [1986*h*].

Morgan and Shemansky [1991] also note that if some of the cometary water is left on the Moon then the subsequent photodissociation of these cooled, or accommodated, gases will yield significantly higher brightnesses within altitudes of several hundred kilometers of the lunar surface. *Morgan and Shemansky* [1991, p. 1357] "simply assume that on average a quarter of the incident water is retained, and note that there is a very large uncertainty in this number." *Frank et al.* [1986*h*] assume that none of the hot postimpact water is injected into or accommodated by the lunar surface.

The lower limits for the brightnesses of OH 308.5-nm and 0 I 130.4-nm emissions from the lunar impacts of small comets are those given above for water as the postimpact gas. As pointed out by *Feldman and Morrison* [1991], the most sensitive search for lunar-associated 0 I emissions is reported by *Fastie et al.* [1973] with the large ultraviolet spectrometer on board Apollo 17. Figure 2 of *Fastie et al.* [1973] we find that the 2σ value for the upper limit of column emissions viewed along a line of sight just above the lunar limb is ~0.08 R. From our above discussion the corresponding lower limit from small-comet impacts is ~0.1 R, a value that is not sufficiently high to be decisive in

TABLE 2. Assumed Physical Parameters for Small Comets

Parameter	*Definition*
$\overline{A}$ = *2%*	albedo of mantle
β_n = 0.1	Knudsen number
C_m = 7.11 *x* 10^6 erg g-r K^{-1}	specific heat of carbon
C_i = 1.67 *X* 10^7 erg g-r K^{-1}	specific heat of water ice
d_g = 2 r_g	intergrain distance
ε = 0.9	thermal ernissivity
f = 0.5	porosity
h = 2cm	mantle thickness
H, = 2.0 *x* 10^{10} erg/g	latent heat of sublimation
K_i = 7 *x* 10^3 erg cm^{-1} s-r K^{-1}	thermal conductivity of water snow
K_c = 15 erg $cm^{-1}s^{-1}$ K-r	contact thermal conductivity of carbon mantle
Pm = 1g/cm^3	bulk density of mantle $\rho_m = (1 - f)\,\rho$ ρ = 2.0 g/cm^3 for carbon
ρ_i = 0.1 g/cm^3	density of water snow
r_0 = ½ r_g	pore radius
r_g = 10^{-4} cm	grain radius
t_m = 5.0	tortuosity of mantle

excluding small-comet impacts because of the uncertainties in computing this estimate. *Feldman and Morrison* [1991] recently examine again the Apollo 17 measurements and derive an upper limit to the 0 I brightness along a 109-km line of sight from the spacecraft to the lunar surface of <0.01 R. However, the scale height for 0 I computed by Morgan and *Shemansky* [1991] exceeds 2 x 10^5 km and the corresponding brightness along a 109-km line of sight is much less than the upper limits given by *Feldman and Morrison* [1991].

The upper limit for OH 308.5-nm emissions associated with the Moon is apparently given by *Hall and Shemansky* [1988*a*] from observations by the IUE satellite. This sensitivity threshold is 30 R. The corresponding estimate for the OH brightness from small comets impacting the Moon is ~70 R (see above discussion).

In summary, the computed brightnesses of OH 308.5nm and 0 I 130.4-nm emissions from small-comet impacts on the Moon are similar to present observational thresholds. For an observer outside of the Earth-Moon system it appears that the brightest emissions at these wavelengths are to be expected from an extended tail of these gases because of grazing impacts with Earth (see section 4.2.2).

Dessler [1991] states that his scaling of the numerical simulation results for comet impacts on the Moon's surface [*O'Keefe and Ahrens,* 1982, p. 371] indicates "an ejecta mass 6 times the comet mass for a 0.1 g/cm³ comet, so 600 tons/min of lunar and cometary material should be injected into lunar-like orbits about the Earth." We agree that there should be some lunar material ejected from the surface by the expanding postimpact gases. The magnitude of the loss of lunar material should be dependent upon the composition and state of the lunar surface. However, most of this dust is not injected into "lunar-like orbits." The escape speed from the Moon's surface is 2.4 km/s, and the escape speed from Earth's gravitational well at the Moon's orbit is 1.4 km/s. Typical gas expansion speeds are expected to be ~4 to 10 km/s [*Frank et al.,* 1986*h; Morgan and Shemansky,* 1991]. A small fraction of the lunar dust from the small-comet impacts is likely to be carried away from the surface at similar speeds by the expanding gases and escapes the Moon's gravitational well. Most of the dust falls back onto the lunar surface. The escaping dust is not expected to be distributed primarily in lunar-like orbits but in heliocentric orbits near the ecliptic plane. For an escape speed of ~5 km/s from the lunar surface the orbital distribution of the dust particles lies primarily in the range of heliocentric radial distances ~0.5 to 2 AU and at low inclinations with respect to the ecliptic plane.

4.2. Interplanetary Water Vapor and Insulation of Small Comets

A small comet is assumed to consist of a core of water snow with a relatively thin mantle of carbon and/or carbon-based material [*Frank et al.,* 1986*d, i,* 1987*c*]. We compute the rate of release of water vapor from such an object in interplanetary space by numercially solving the heat equations for the core and mantle as given by *Fanule and Salvail* [1984]. The assumed physical parameters for the small comets are given in Table 2. All values of the constants in Table 2 are cited by *Fanale and Salvail* [1984] with the exceptions of h, K_c, and ρ_m. The thermal conductivity for the carbon mantle is $K_c = \alpha K$, where a is the hertz factor [*Brin and Mendis,* 1979] and K = 1.5 x10^5 erg s^{-1} cm^{-1} K^{-1} is the bulk conductivity of amorphous carbon. For our present calculations, $\alpha = 10^{-4}$.

Our model differs from that of *Fanale and Salvail* [1984] in the substitution of a thin consolidated mantle of porous carbon bound by cohesive forces for their mixture of water snow and silicate dusts that forms a dust mantle bound by the gravitational force of a much larger comet. Presumably, such cohesive forces between particle grains can exist in the same manner as those for clay particles as previously suggested by laboratory experiments [*Storrs et al.,* 1988]. Laboratory irradiation of methane ices also supports the assumption of carbon-based mantles [*Lanzerotti et al.,* 1985; *Johnson et al.,* 1986]. Otherwise for the small comets, gravity is unable to support a mantle against the pressure of the water vapor from the core. In addition, because the cometary mass is small relative to that of large comets, the numerical simulation includes the temperature changes of the core along the trajectory.

The computed maximum temperature for the mantle surface and the temperature of the core-mantle interface for a small comet moving along a sun-approaching trajectory are shown in Figure 6. The rotational period of the small comet is 2400 s and the obliquity is 90°. The mantle thickness is 2 cm. Perihelion for the orbit is 0.9 AU. At 1 AU the maximum mantle temperature is 389 K and the mantle-core interface temperature is 165 K. With decreasing heliocentric radial distances these temperatures rapidly increase in such a manner that it is unlikely that many small comets reach the orbit of Venus (0.72 AU) [*Frank et al.,* 1986*c, e*]. Perihelia of most of the small comets are assumed to be $\gtrsim$ 0.9 AU. If the integrity of the mantle of a small comet is flawed by a crack or puncture, it is expected that catastrophic disruption occurs and hence that the small comet cannot endure a long series of successive orbits. We note that the images of comet P/Halley from the Giotto flyby show that this large comet exhibits a mantle of nonvolatile material with very low geometric albedo and with only small active areas providing the gases and dust in the coma [*Keller et al.,* 1986]. Perhaps these breaches of the mantle are due to impacts from smaller interplanetary objects.

The water vaporization rate averaged over the surface of a small comet is also shown in Figure 6. At 1 AU this vaporization rate is 6 x 10^8 H_2O molecules cm^{-2} s^{-1}, less than the upper limits previously determined by other considerations [*Frank,* 1986*d; Donahue,* 1987]. For comparison, the vaporization rate for bare, pure water ice at 1 AU is ~3 x 10^{17} cm^{-2} s^{-1}. Total mass loss per orbit for the small comets is $\lesssim$ 10 g. Thus small comets with 2-cm mantles in orbits with perihelia $\gtrsim$ 0.9 AU can be long-lived and survive a large number of perihelion crossings. We note that the

corresponding computed vaporization rates at 1 AU for mantle thicknesses of 1 and 3 cm are 7 x 10^{10} and 2 x 10^{7} cm^{-2} s - l, respectively.

For the present numerical calculation the comet mass is 10^{8} g. The vaporization rates for a smaller mass of 2 x 10^{7} g with the same density are roughly proportional to the surface area of the mantle, i.e., factors of 2 to 3 lesser than the rates shown in Figure 6. These water vaporization rates are much more steeply dependent upon the physical properties of the mantle.

1. *Morris* [1986] and *Frank et al.* [1986i] do not provide a quantitative estimate of the fraction of the small comets that are scattered into retrograde orbits by Jupiter and hence enter Earth's atmosphere with high speeds. *Dessler* [1991, p. 372] miscites *Frank et al.* [1986*i*] in stating that "one sixth of the small comets are in retrograde orbits" in order to base his claim that at least two bright, high-speed impacts should be seen each night by a ground observer. No such statement is made by *Frank et al.* [1986*i*].

However, the anticipated orbital distribution of the small comets is an important topic. *Frank et al.* [1987*c*] [also *Frank and Craven,* 1988; *Frank,* 1989] propose that the source of the small comets is an Oort disk lying generally near the ecliptic plane and beyond the orbits of the known planets [*Oort,* 1950; *Hills,* 1981]. Gravitational deflection by a large body passing through the disk scatters some of the small comets into highly eccentric, prograde orbits with perihelia inside the planetary system and lying near the ecliptic plane.

Subsequent gravitational action of the large, outer planets, in particular that of Jupiter, must be considered. The semimajor axes of these initially long-period comets are rapidly changed with each transit of the planetary system, $\Delta E \simeq -4.5 \times 10^{-4}\ AU^{-1}$ [*Everhart,* 1968] In order to account for the large flux at Earth, a substantial fraction of the long-period comets must be captured into short-period orbits. Direct capture by Jupiter is insufficient to yield a substantial number of short-period comets [*Newton,* 1893; *Everhart,* 1969]. In order to account for the relatively large number of observed short-period comets (large) in prograde, low-inclination orbits, *Everhart* [1997] (also cited by *Fernández* [1980]) calculates the capture rate for many successive orbits through the planetary system. The fraction of such comets that are captured is $\sim 10^{-2}$ and the average corresponding orbital period is $\simeq$ 7 years for perihelia 0 to 5.8 AU. Thus a population of objects in prograde, short-period orbits near the ecliptic plane is established. The remainder of the initial population is scattered out of the planetary system along hyperbolic orbits. This same mechanism can provide a prograde stream of small comets at Earth's orbit and requires the anticipated long lifetime of the small comets against vaporization.

2. The proposed mode of breakup of a small comet (see section 2.1) suggests that the carbon or carbon-based mantle is reduced to small grains and dispersed throughout the cometary water cloud before impact with Earth's atmosphere. It is thus likely that much of the carbon is oxidized in the atmosphere, forming CO and CO_2, rather than appearing as

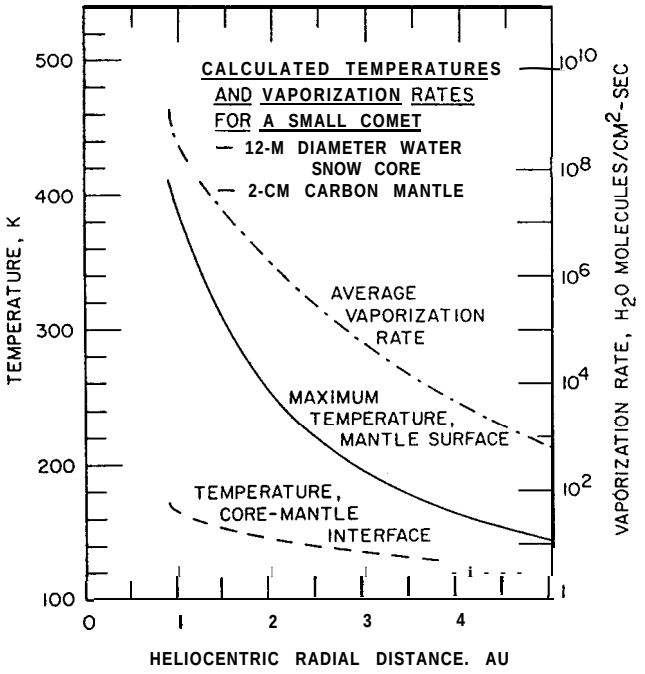

Figure 6. Calculated temperatures and water vaporization rates for a small comet with a 0.1 g/cm^3 water snow core and a 2-cm carbon mantle as a function of heliocentric radial distance as the comet approaches the Sun. The mass of the water snow core is 10^{8} g for this example.

soot precipitation on Earth's surface [*Frank et al.*,1986*i*]. Perhaps the best upper limit for an extraterrestrial source of carbon is provided by the estimates of global carbon cycling. Utimately, the cometary carbon is expected to be deposited in Earth's crust in the form of sedimentary rocks. *Holland* [1984] determines that the total amount of carbon in the crust is ~9 x 10^{22} g and that ~3.4 X 10^{14} g of carbon is buried each year in sedimentary rock. Approximately 75% of this carbon is provided by weathering of old sedimentary rocks, and the remainder, ~8(± 3) X 10^{13} g, is believed to be due to carbon released from the metamorphism of sedimentary rocks and by juvenile carbon from the mantle. This latter rate, ~10^{14} g/yr, is taken here as a crude upper limit to the carbon influx from small comets. For the model comet presented earlier in this section the corresponding carbon flux is ~10^{14} g/yr. However, the wide possible ranges of assumed parameters, for example, diameter, mantle thickness, chemical composition, and mechanical properties, preclude use of the terrestrial carbon budget as a decisive observation for or against the existence of the small comets.

The high luminosity associated with the impact of a stony or iron meteoroid with Earth's atmosphere is due in large part to relatively low excitation and ionization energies of meteoric metallic atoms and to allowed transitions that yield emissions at visible wavelengths [cf. *Öpik,* 1958; *Bronshsten,* 1983]. The excitation energies of cometary atoms such as H, C, 0, and N are relatively high and the corresponding radiation yields are low [*Bronshsten,* 1983]. Estimates of the visual brightness of the impact of a small comet with Earth's atmosphere depend upon a realistic, and as yet unavailable,

numerical simulation of this complex event (see section 3.1.1).

4.2.1. **Hydrogen torus at 1 AU.** *Frank et al.* [1986*d*] derive an upper limit for the water vaporization rates from the surfaces of the small comets at a heliocentric radial distance 1 AU from an upper limit for pickup ion densities in the solar wind. This upper limit is in the range of 3×10^{10} to 3×10^{11} H_2O molecules $cm^{-2} s^{-1}$. By using Voyager 1 and 2 observations of interplanetary Lyman a radiation, *Donahue* [1987] provides an upper limit for the vaporization rate of $\sim 1.3 \times 10^{9}$ $cm^{-2} s^{-1}$. The corresponding upper limit for the solar Lyman α radiation scattered by an inner solar system source of hydrogen from the photodissociation of cometary water is ~25 R. After a further analysis of the Voyager 2 data, *Donahue et al.* [1987] find an excess component of Lyman a radiation relative to the background radiation due to hydrogen from the interstellar wind. This excess radiation from measurements near 1 AU is ~163 R. However, *Hull and Shemansky* [1988*b*] show that the excess component of Lyman α radiation near 1 AU as reported by *Donahue et al.* [1987] is simply a manisfestation of the viewing geometry. The upper limit for the excess radiation as derived by *Hull and Shemansky* [1988*b*] is ~20 R. The corresponding upper limit for small-comet vaporization rate is $\sim 10^{9}$ H_2O water molecules $cm^{-2} s^{-1}$. The Voyager 2 observations are very limited: seven' observations at ~1 AU and the next reported one (no excess radiation) at ~1.3 AU. Determinations of a cometary source of atomic hydrogen in the inner solar system are made difficult by the viewing dependence of the background glow due to the presence of the interstellar hydrogen at larger heliocentric distances, ~150 to 700 R [*Ajello et al.*, 1987], and by the variability of the solar Lyman α radiation.

Insight into the relationship of scattered Lyman a intensities from hydrogen arising from a source of interplanetary water and the presence of small comets can be gained by examination of Figure 6. For this model of a small comet the water vaporization rate is $\sim 6 \times 10^{8}$ H_2O molecules $cm^{-2} s^{-1}$ at 1 AU and decreases by a factor of 10 at 1.3 AU. The distribution of cometary water and photodissociated hydrogen atoms is concentrated in a torus around the Sun near the ecliptic plane because of the low inclinations of the small-comet orbits. A coarse estimate of the Lyman a radiation from the cometary water can be obtained. For a small-comet spatial density of 10^{-25} cm^{-3} and a comet radius of 600 cm, the source S of hydrogen is $\sim 3 \times 10^{-10}$ H atom $cm^{-3} s^{-1}$. The equilibrium density of atomic hydrogen, ρ, is given by $S = \rho/\tau$, where τ is the charge exchange lifetime for hydrogen in the solar wind. The scattered solar Lyman α intensity at 1 AU in a direction perpendicular to the vector to the Sun and parallel to the ecliptic plane is $4\pi I \simeq 10^{-6} g \rho L$ in Rayleighs (R), where L is the characteristic radial thickness of the torus, taken here as 0.3 AU. For the quiet Sun the g factor is $\sim 1.4 \times 10^{-3} s^{-1}$ and τ is $\sim 2.4 \times 10^{6}$ s at 1 AU [*Opal and Carruthers*, 1977]. Then the density of atomic hydrogen at 1 AU is $\sim 7 \times 10^{-4}/cm^3$ and the scattered solar Lyman α intensity is ~5 R.

In order to determine whether or not there is a hydrogen torus around the Sun due to the water vaporization from small comets an accurate characterization of the larger background intensities due to the presence of interstellar hydrogen must be acquired. The extensive survey of interplanetary Lyman α radiation with the ultraviolet spectrometers on Galileo [*Hord et al.*, 1992] offers the most comprehensive search for a dim hydrogen torus at heliocentric radial distances ~1 AU.

4.2.2. **Earth as a comet.** *Dessler et al.* [1990] point out that some small comets travel along trajectories with closest-approach distances inside the breakup altitude but higher than altitudes sufficient to slow the disrupted cometary water. Thus such small comets produce a more or less conical tail of H_2O and its dissociated products, H, 0, and OH, with axis directed along Earth's orbital velocity vector. *Dessler et al.* [1990] calculate that the maximum brightness of the O-O band of OH at 308.5 nm due to fluorescence from solar radiation is ~5 kR as viewed outward along the axis of the tail from positions $\lesssim 120 R_E$ from Earth's surface. This computed brightness is too large for two reasons: (1) the assumed breakup altitude of ~3200 km is too high (see section 2.1) and (2) telescopic observations indicate that the typical mass of a small comet is $\sim 2 \times 10^{7}$ g, not the $\sim 10^{8}$ g originally inferred by *Frank et al.* [1988*b*] (see section 5.2.1). For a more plausible breakup altitude of 1000 km and lesser cometary mass the corresponding brightness is reduced by a factor of ~25 to ~200 R. Each adjustment 1 and 2 above contributes about equally to this reduction, i.e., a factor of ~5. The Galileo ultraviolet spectrometer [*Hord et al.*, 1992] offers the best current opportunity to observe the cometary tail during this spacecraft's two close flybys of Earth for orbital assists to Jupiter during December 1990 and December 1992. The ~200-R brightness of the tail at 308.5 nm is near the observational limits of the Galileo ultraviolet spectrometer (C. Hord, private communication, 1991).

5. OTHER EVIDENCE

Three topics are discussed by *Dessler* [1991] in this section: (1) the detection of atmospheric holes in clusters of pixels in the Viking images of ultraviolet dayglow, (2) the sightings of small comets with the Spacewatch Telescope at Kitt Peak National Observatory, and (3) the visibility of small comets after breakup with the naked eye of a ground observer. Detections of upper atmospheric water bursts with a microwave radiometer are omitted by *Dessler* [1991] (see section 3).

5.1. Atmospheric Holes-Viking Results

Dessler [1991] states that the detection of atmospheric holes in the Viking Images as reported by *Frank et al.* [1989] is not statistically significant. A possible example of an atmospheric hole is to be found in the Viking image shown in Plate 2. The spectral passband of the instrument is similar to that used for the Dynamics Explorer 1 images of atmos-

pheric holes. Because of the very limited number of Viking images of Earth's dayglow, few such detections are available, and a rigorous statistical analysis of their significance is necessary. In addition, laboratory calibrations are ambiguous as to whether these dark spots are due to instrumental effects as noted in the original paper by *Frank et al.* [1989] and later by *Cragin* [1990] and *Dessler* [1991]. Obviously, an inflight calibration is required in order to eliminate instrumental effects as the source for the apparent atmospheric holes in the Viking images.

The required inflight calibration is reported by *Frank et al.* [1989]. Consider the Viking image in Plate 2 and the Dynamics Explorer 1 image in Plate 1. The spectral passbands are broad and include the optically thick 0 I 130.4-nm triplet, together with the optically thin 0 I 135.6-nm lines and N_2 Lyman-Birge-Hopfield (LBH) bands. When viewing the Earth's atmosphere in the nadir direction, the principal contributor to the responses of the imagers is emissions at 0 I 130.4 [*Anderson et al.*, 1980; *Meier et al.*, 1980]. However, as the viewing angle from nadir increases, the relative contributions from the 0 I 135.6 and N_2 LBH emissions increase. Examination of the cross section for water vapor [*Watanabe and Zelikoff*, 1953] reveals an important feature: the total absorption cross section for water vapor has a broad minimum spanning the spectral range of the 0 I 135.6 and N_2 LBH emissions that is a factor $\gtrsim 3$ lesser than that for 0 I 130.4. In other words, atmospheric holes should be observed in generally nadir directions but not near the atmospheric limb where the large optical paths provide limb brightening of the 0 I 135.6 and N_2 LBH emissions for which the water absorption cross section is relatively small. This effect is observed in the Dynamics Explorer 1 images.

Thus the source of the apparent atmospheric holes in the Viking images can be identified as (1) instrumental or (2) geophysical by using inflight images to determine their occurrence rates in nadir- and limb-viewing directions. If the apparent holes occurred with equal frequencies in the nadir- and limb-viewing directions, then their source is instrumental. On the other hand, if the holes are found primarily in nadir-viewing directions, their appearance in the images is clearly related to a geophysical effect. *Frank et al.* [1989] define a simply derived fluctuation parameter E for 3 x 3-pixel blocks in the Viking images. In contrast to the occurrence of most of the atmospheric holes as single pixels in the Dynamics Explorer 1 images, these events occur as cluster of typically 5 to 7 pixels in the Viking images. These 3 x 3-pixel blocks are then separated into two groups: nadir-viewing and limb-viewing. The two normalized occurrence probabilities are shown as a function of E in Figure 7. Events with lower values of log E are the darker events. For values of log $E \leq -16$ there is a significant difference in the two distributions: seven events for nadir-viewing pixels and one event for limb-viewing pixels. *Frank et al.* [1989] find that the probability for all seven nadir events to be random is 9×10^{-5}.

To our knowledge, *Cragin* [1990, p. 1174] provides the only published evaluation of the statistical significance of

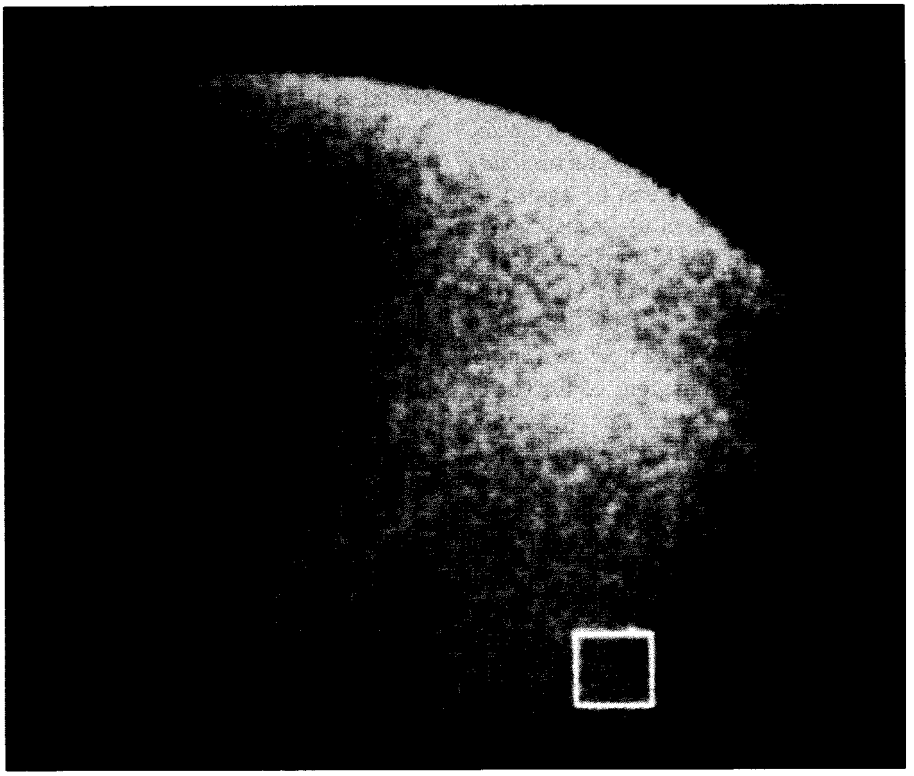

Plate 2. Viking image of a transient decrease of ultraviolet dayglow intensities over the northern hemisphere at 0052 UT on April 29, 1986 [*Frank et al.*, 1989]. The brighter areas of the image are near or at saturation values of the sensor and thus are not usual in the search for atmospheric holes.

the Viking events, other than the papers by *Frank et al.* [1989, 1990*a*]. Cragin finds "Nevertheless it (the random probability) is still small enough that---were it not for an additional reservation to be considered in the following section-one could conclude that the observed 7 to 1 partitioning of events is in fact statistically significant at the 95% confidence level." Cragin's reservation is the subjective conclusion "To my eye, no evidence remains in this figure (his edited version of Figure 7) of a separation at log $E = -16$ of the nadir-viewing distribution into two distinct statistical populations, one well-behaved and the other anomalous." In their reply, *Frank et al.* [1990*a*] confirm Cragin's rigorous conclusion that the nadir-viewing events are statistically significant and advance the corresponding confidence level to 99.6% by including the entire set of previously reported 3 x 3-pixel blocks.

Occurrence frequencies, intensity decreases, and dimensions of the clusters of darkened pixels in the Viking images are similar to those previously reported for atmospheric holes as seen in the dayglow images from Dynamics Explorer 1 [*Frank et al.,* 1989, 1990*a*].

5.2. Direct Detection

Yeates [1989] reports the first successful search for small comets with a ground-based telescope. The naked-eye visibility of the cometary water cloud that is formed after breakup at low altitudes depends critically upon the physical state of the cometary debris.

5.2.1. **Optical detection.** *Dessler* [1991, p.374] states that "Soter performs a retrospective analysis of telescopic data acquired by *Taff* [1986] before the small-comet hypothesis was advanced." On the other hand, *Yeates* [1989, p. 1185] notes that "*Soter* [1987] has previously claimed that the detection of these small comets should be possible with the M.I.T. space surveillance telescope that is the prototype for the GEODSS systems. However this claim was not supported by a detailed analysis of the telescope's capabilities or by an observational campaign." In other words, there is no analysis of telescopic images by *Soter* [1987]. However, the paper by *Soter* [1987], and the works of *Stewart et al.* [1986] and *Frank et al.* [1987*a*], provide the motivation for the first successful telescopic detections by *Yeates* [1989].

Yeates [1989] uses a specially designed operating mode to optimize the probability of detection of small bodies in the vicinity of Earth with the Spacewatch Telescope at Kitt Peak National Observatory [*Gehrefs and Vilas,* 1986; *Gehrels et al.,* 1986]. The viewing geometry is shown in Figure 8. His scheme is based upon finding the slew rate of the telescope such that the object dwell time on a pixel of the charge-coupled device (CCD) array at the focal plane is optimized (S/N ontimized) and, at the same time, to maximize the volume for detection of the objects. The corresponding slew rate is a function of the telescope collecting area and the characteristics of the CCD. By chance this slew rate is the sidereal angular rate, 73 μrad/s. The viewing range is centered at ~137,000 km. This "skeet-shooting" scheme is necessarily performed near the noise level of the telescope and

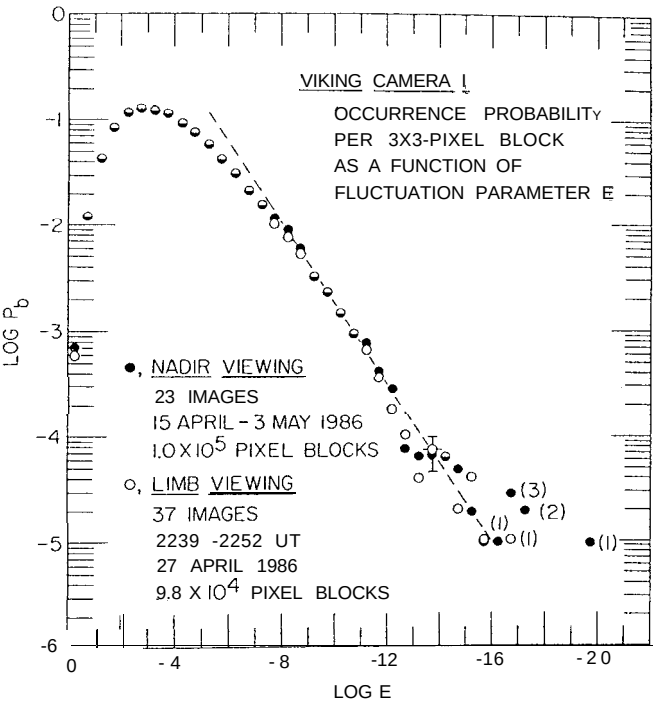

Figure 7. Normalized probability P_b for 3 x 3-pixel blocks of the Viking dayglow images as a function of fluctuation parameter E. Numbers of events are shown in parentheses [*Frank et al.,* 1989].

at favorable solar phase angles of ~160°. This observing technique depends critically upon knowledge of the orbital parameters of the small bodies; and the orbits for small comets given by *Frank et al.* [1986*b, i,* 1987*a*] are used as targeting parameters. These orbits are highly eccentric with perihelia ~1 AU, prograde, and near the ecliptic plane.

Because there is only a very small probability that the objects are perfectly tracked by the telescope (see Figure 8) their trails appear as dim streaks in the images and extensive analyses are required. *Yeates* [1989] identifies 33 trails of small bodies in 171 images from the Spacewatch Telescope taken during November 1987 and January 1988. The apparent visual magnitudes of the objects range from $18^m.7$ to $18^m.0$. The probability that the individual trails are random events ranges from one event in 10^3 images to one event in 10^{12} images. The trails are not due to random fluctuations in the pixel responses of the CCD. *Yeates* [1989] considers and eliminates other causes for the observed trails: Earth-orbiting debris, meteors, cosmic rays, and β particles from the natural radioactivity of the CCD substrate.

Only one image of a given small body is obtained in the search by *Yeates* [1989], i.e., the "first image" in Figure 9. In order to confirm the detection of these objects the search technique is extended to two consecutive images of the same object with observations taken by T. Gehrels during April 1988 [*Frank et al.,* 1990*b*]. As shown in Figure 8, the exposure time for the first image is 12 s, which is followed by an interval of 36 s for readout of the image before the 12-s exposure time for the second image. The telescope tracks the object at a constant slew rate for this sequence of

events. The criteria for identifying the same object in consecutive images are greatly restrictive. The two trails must have the same length and brightness and be collinear with a separation of three trail lengths.

A total of 48 pairs of consecutive images are available from the observing campaign on April 19, 1988, with the Spacewatch Telescope [*Frank et al.,* 1990*b*]. An example of detection of the same body in two consecutive images is shown in Figures 9 and 10. Various artifacts are identified in the first image, including CCD defects, cosmic rays, and dust on the telescope optics. Star trails are all of the same length as the telescope field of view moves across the star field during the search mode. The trail of a small body is shown centered in the box. The trail of the same small body during the second exposure is identified in Figure 10. In order to confirm that these trails satisfy the stringent criteria for detection of the same object in two consecutive images, residual pixel maps of the two trails are constructed as shown in Figure 11. These residual responses are computed by subtracting the background, typically ~140 dn (digitization units), from the observed pixel responses. The fluctuations in the pixel responses along the two trails exhibit the statistical fluctuations expected from these low-response levels

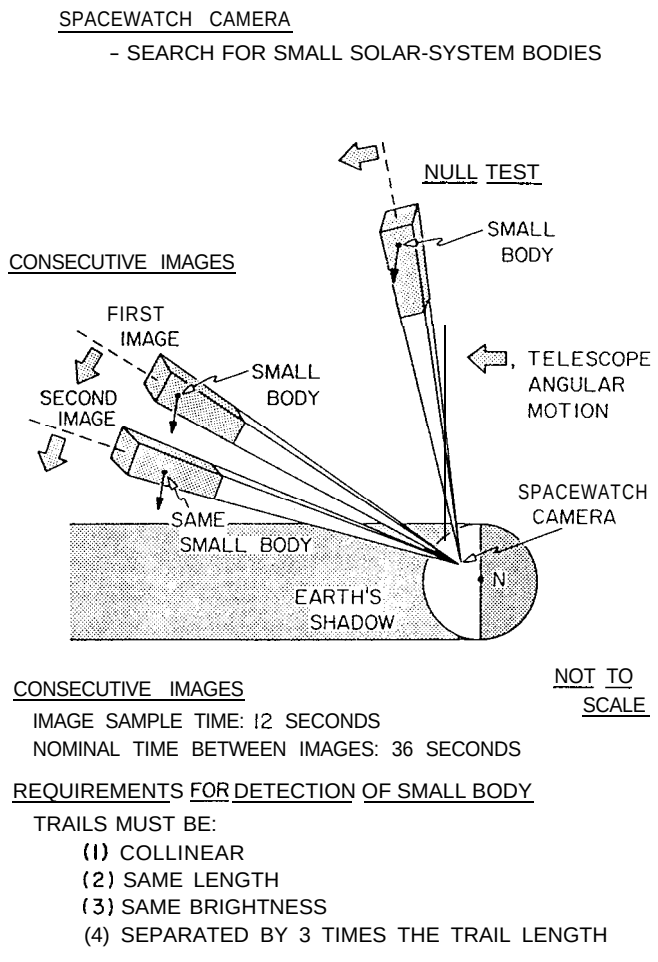

Figure 8. Viewing geometries for the Spacewatch Telescope for the acquisition of consecutive images of the small comets and for the null test on April 19, 1988 [after *Frank et al.,* 1990*b*].

and are similar to those for the faint star trail identified in Figure 9.

Because the consecutive images reveal only pairs of trails that satisfy the criteria for detection of the same object, except when a trail is obscured by a star or is positioned outside of the telescope field of view, only an upper limit for the appearance of such random pairs of trails can be obtained [*Frank et al.,* 1990*b*]. This upper limit is obtained by assuming that all of the trails are random events. Then the probability that the pair of trails shown in Figure 11 is a random event is once each 8 billion pairs of image frames. Note that only 48 pairs of consecutive images are available. Clearly, small bodies are being detected by the Spacewatch Telescope. Six small bodies in this series of consecutive images are reported by *Frank et al.* [1990*b*], with upper limits for random occurrence ranging from once each 1 million to once each 10 billion image pairs. The apparent visual magnitudes are similar to those previously reported by *Yeates* [1989].

The viewing geometry for a null test for the small-body trails is shown in Figure 8. These images are taken at solar phase angle 80". No trails due to these small bodies are expected in the images because of the increase in their apparent angular motion (longer trails) and decrease in their phase function (lesser brightness). No trails are found in the 38 image pairs [*Sigwarth,* 1989; *Frank et al.,* 1990*b*].

A more comprehensive examination of the 48 pairs of consecutive images by *Sigwarth* [1989] yields 24 pairs of small-body trails. The apparent visual magnitudes range from $19^m.5$ to $18^m.2$. The average volume for detection of these objects with the Spacewatch Telescope is ~9 x 10^9 km^3 (see Figure 8). With assumed values for-the reflectance parameter p, mass density p and phase law ϕ an integral number density of these small bodies as a function of mass M can be calculated. This mass spectrum is shown in Figure 12. Phase law ϕ is taken as 0.25 [*Lumme and Bowell,* 1981*a*, *b*]. Three mass spectra are shown in Figure 12 that correspond to three possible combinations of p and p. The corresponding spatial densities of small comets as deduced from observations of atmospheric holes from Dynamics Explorer 1 are also shown. Maximum, minimum, and average densities are derived from the temporal variations of the occurrence rates of atmospheric holes [*Frank et al.,* 1987*a*]. It is evident that the integral mass spectrum from the telescopic observations is very steep and flattens at low masses. Second, the masses of these small comets are very probably less than the values originally estimated by *Frank et al.* [1986*b*] from observations of atmospheric holes, i.e., ~10^8 g. The expectation for mass from the telescopic measurements is ~2 x 10^7 g with an uncertainty in the range of a factor of 3.

Because of the small size, and hence lesser apparent visual magnitude, of the small comets as detected by the Spacewatch Telescope relative to the predictions by *Frank et al.* [1986*b*, *i*, 1987*a*], the trails in the telescopic images are dimmer than expected for the original telescopic search. The tuning distance for the Spacewatch Telescope can be adjusted to observe the objects at closer distances, and hence with

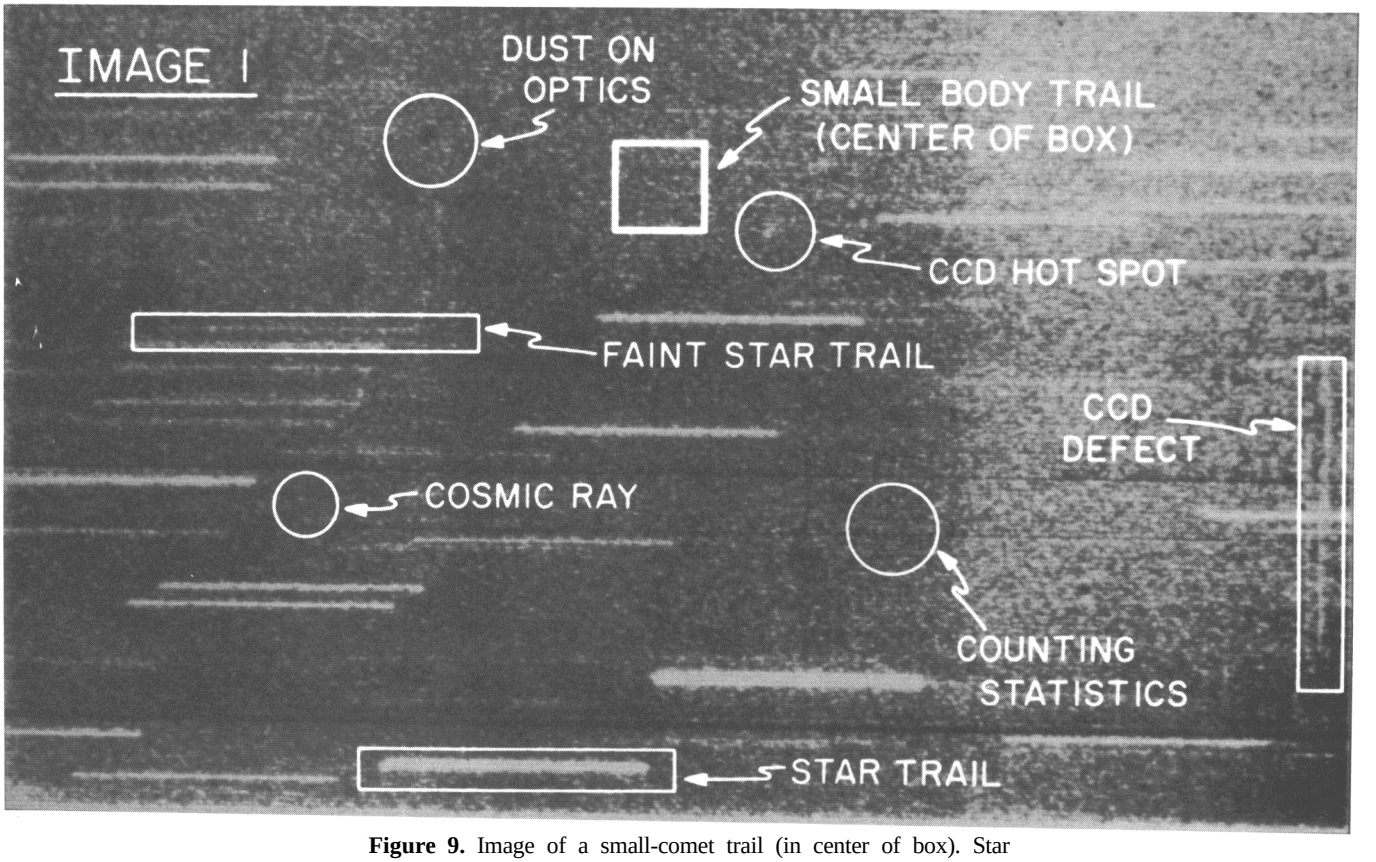

Figure 9. Image of a small-comet trail (in center of box). Star trails and various instrumental artifacts are also identified. The exposure time is 12 s [after *Frank et al.,* 1990*b*].

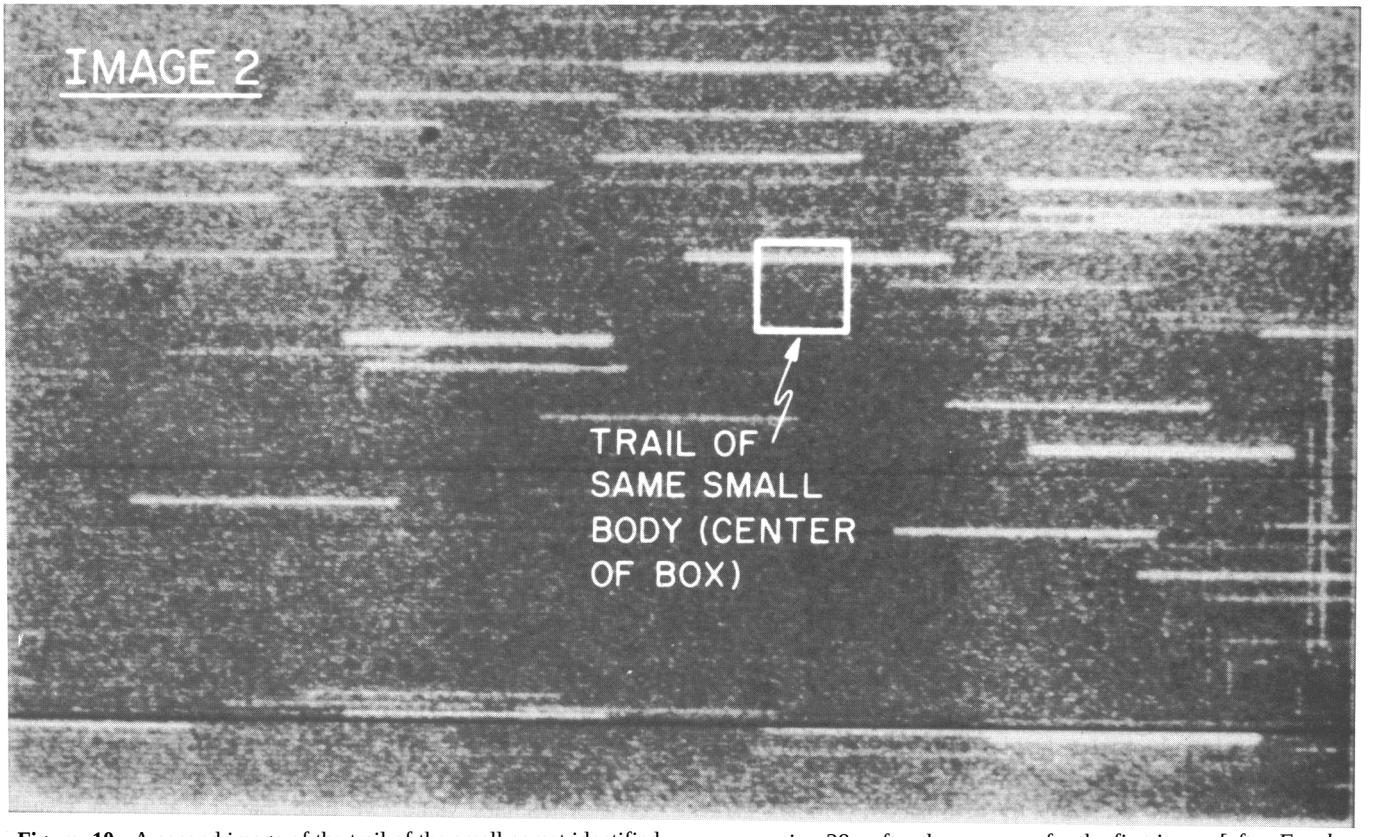

Figure 10. A second image of the trail of the small comet identified in Figure 10. This image was obtained during a 12-s exposure commencing 38 s after the exposure for the first image [after *Frank et al.,* 1990b].

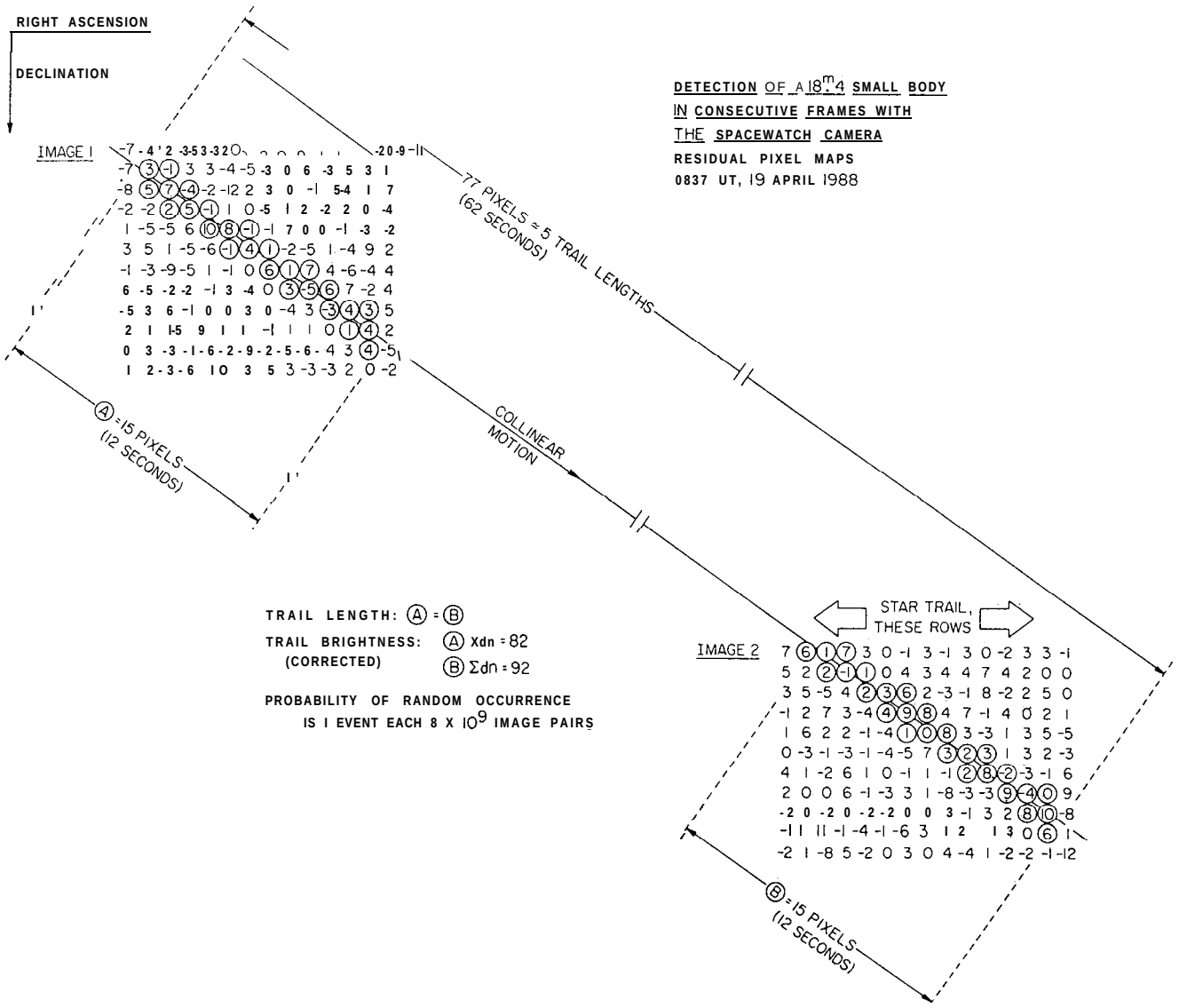

Figure 11. Pixel maps for the two trails of Figures 9 and 10 in the coordinate system of the array detector [after *Frank et al.*, 1990*b*]. Residual responses above the average background are shown. The two trails satisfy the stringent requirements for detection of the same object in consecutive frames: trails are (1) same length, (2) same brighter, (3) collinear, and (4) separated by three trail lengths.

brighter trails. For example, for a $1^m.0$ increase in apparent visual brightness, and a factor of ~2.5 increase in pixel responses, the tuning distance can be set at ~86,700 km. This distance corresponds to an angular scan rate with respect to the celestial sphere of ~110 μrad/s, (i.e., leading Earth's rotation by ~40μrad/s). However, the detection volume (see Figure 8) decreases severely with decreasing tuning distance [*Yeates*, 1989], and the detection rate per frame is less by a factor of ~4.

The reduced mass estimate is important in assessing the physical state of the water vapor responsible for the transient absorption of ultraviolet dayglow observed as atmospheric holes with Dynamics Explorer 1. Specifically, the mass of the small comets is originally estimated by *Frank et al.* [1986*b*] with the assumption that the water vapor in the obscuring cloud is composed of unbound water molecules. As discussed in section 2, the content of the water vapor cloud may consist of dimers and molecular clusters, in which case the ultraviolet absorption cross section is expected to increase significantly with respect to the corresponding multiple of the single-molecule cross section. The mass of water vapor required to produce an atmospheric hole is correspondingly reduced to values in the range of the masses from the direct telescopic sightings.

5.2.2. **Visual detection.** The brightness of a small comet after fragmentation is a subject of considerable interest because of the possibility of visual detection by a ground observer positioned at predawn or postdusk local times while the ice cloud is illuminated by sunlight at higher altitudes. As a benchmark value, we note that the apparent visual magnitude of the small comets just prior to breakup at an altitude of ~1000 km is $M_v \gtrsim 8^m$ if we use the telescopic

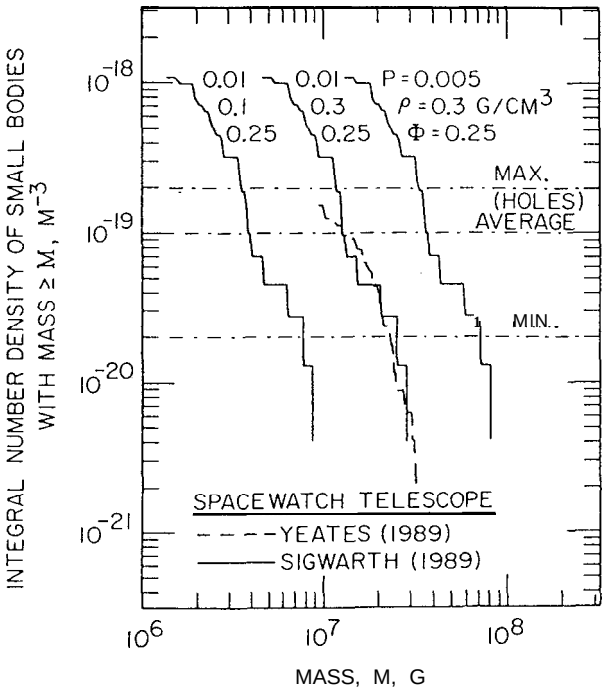

Figure 12. Integral number densities of small comets as a function of mass as derived from observations of their apparent visual magnitudes with the Spacewatch Telescope [after *Sigwarth,* 1989]. Three mass spectra are shown for three assumed sets of values for reflectance parameter p and mass density p. The minimum, maximum, and average densities as derived from observations of atmospheric holes with Dynamics Explorer 1 are also indicated.

detections of these objects at a range of ~137,000 km as reported by *Yeates* [1989] and *Frank et al.* [1990*b*]. During the brief interval at breakup when the mantle is stripped and prior to significant outflow of core material, the corresponding range of visual magnitudes is estimated as 4^m to 2^m. The visual threshold for meteors is $M_v \simeq 5^m$.

The brightness of the cloud of ice grains after fragmentation of the small comet is highly dependent upon the detaih of their sizes and dispersal. For reasons of geometric simplicity we assume that the maximum brightness of the ice cloud occurs when 90% of the cometary contents (1.8 x 10^7 g) are dispersed uniformly as ice crystals into a disk with radius 1 km and with axis along the viewing direction of the ground observer. The range of this disk is 1000 km. If the contents are 20μ (radius, *r),* spherical ice crystals, then the ice cloud is bright as a result of Mie scattering [cf. *Hansen and Travis,* 1974] because the size parameter $2\pi r/\lambda \simeq 230$ is large. The apparent surface brightness of the cloud is ~450 erg $cm^{-2} s^{-1}$ sr^{-1}. For comparison, the brightness of the full Moon is ~2 x10^4 erg $cm^{-2} s^{-1} sr^{-1}$ and that of the clear sky at local sunrise and sunset is ~20 erg $cm^{-2} s^{-1} sr^{-1}$ [*Rozenberg,* 1966]. The apparent visual magnitude of the ice cloud is about $-5^m.3$, and because its apparent angular size is small, ~ 7 arcmin, it briefly mimics brightest Venus ($-4^m.4$).

On the other hand, the surface brightness from a cloud of water clusters is due to Rayleigh scattering. The entire small-comet mass of 2 x 10^7 g is assumed to be dispersed into a similar disk (radius, 1 km) of water clusters ($r \simeq 5 \times 10^{-8}$ cm, or ~17 H_2O molecules). The cloud is assumed to be optically thin and the scattering approximated by that for spherical dielectric spheres [cf. *van de Hulst,* 1957; *Liou,* 1980]. This surface brightness is ~7 x 10^{-2} erg $cm^{-2} s^{-1}$ sr^{-1} and varies as r^3. The apparent visual magnitude of the ice cloud is then $\sim 4^m$.

The full angle for the field of view for a ground observer is typically ~40°. *McKinley* [1961] provides a thorough discussion of the visibility of meteors with the naked eye. The frequency of small-comet breakups within this field of view is approximately one each 1.5 hours. This event frequency is to be compared with that observed for meteors with $M_v \leq 4^m$, ~24 events for the same time interval of 1.5 hours. A moving object with $M_v \simeq 4^m$ is near the threshold of detection by the human eye. It is estimated that ~0.1% of these objects are detected within the field of view of the naked eye [*McKinley,* 1961, Figure 5-1]. Thus, not only is naked eye detection of the contents of the fragmented small comet made difficult by the presence of a substantially greater rate of meteors of the same magnitude but the rate of detection of these events is roughly one per 1500 hours of viewing. This latter viewing, of course, is with the observer in darkness and the cometary cloud exposed to sunlight, a period of about 3 hours per day at mid-latitudes.

The purpose of the above discussion is to describe a reasonable physical state for the snowy core of a small comet and a subsequent mode of dispersal of this material that does not produce a very bright glow in the sky. This possibility is in direct contradiction to the quantitatively unsupported claim by *Dessler* [1991] that the dispersed icy contents of a small comet must be a strikingly bright event to the naked eye.

6. THE INSTRUMENT-ARTIFACT HYPOTHESIS

Dessler [1991] bases his conclusion that atmospheric holes are instrument artifacts on consideration of (1) the observed motions of atmospheric holes across the sunlit Earth, (2) the diurnal variations for atmospheric holes, (3) the temporal variations of this phenomenon, and (4) expectations for the sizes of atmospheric holes as seen from low altitudes. This latter topic includes the topic of darkening of pixels adjacent to an atmospheric hole as seen from higher altitudes.

The reader is reminded that the imager is a spin-scan photometer [*Frank et al.,* 1981]. A scan line across the face of Earth is acquired during a spacecraft spin period of 6 s. The effective field of view for each pixel in this scan line is 0.29°. The separation of the centers of two adjacent pixels is 0.23° in angle and 3.8 ms in time. An internal mirror in the instrument, i.e., the scanning mirror, is rotated such that the next scan line is acquired at an angular displacement of 0.25° from the preceding scan line. A partial pixel map of an image is shown in Figure 13. This map is centered on an atmospheric hole that is seen in three adjacent scan lines (see Plate 1). Two of these pixels display decreases of dayglow

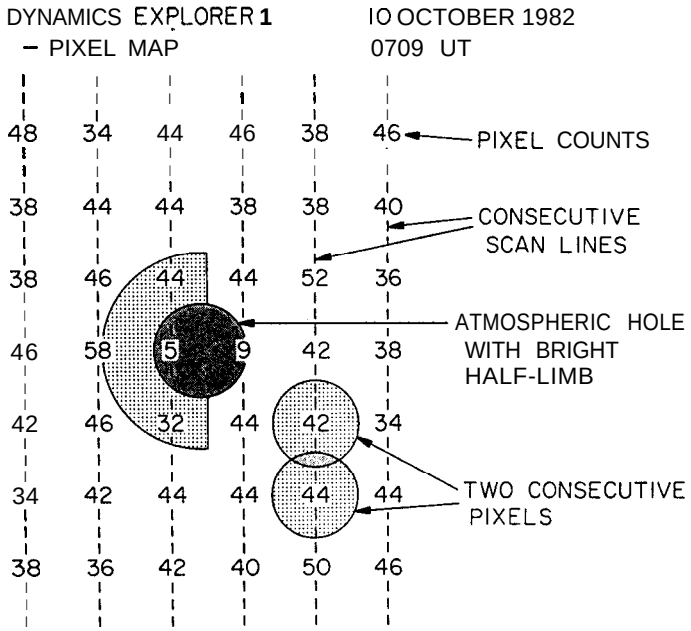

Figure 13. Pixel responses for the atmospheric hole shown in the inset of Plate 1. The overlap between two consecutive pixels in a scan line is also shown. The scan lines advance from right to left [after *Frank et al.,* 1987*b*].

intensities, the third pixel displays an intensity enhancement. The scan lines are being acquired from right to left in the image, which corresponds to motion from east to west, i.e., from local evening toward local morning, across the face of Earth. The speed of the object perpendicular to the line of sight is ~11 km/s if its altitude is ~1000 km. That is, the scanning mirror is fortuitously tracking the object.

Frank et al. [1986*g*] find that most of the atmospheric holes that are tracked in adjacent scan lines are moving in the east-to-west direction. Because such observations depend only upon the scan direction of the instrument mirror it is very difficult, if not impossible, to identify these motions as an instrument artifact. Such motion is consistent with objects in prograde, low-inclination orbits with perihelia near Earth's orbit and aphelia at and beyond Jupiter's orbit. A fraction, ~20%, of the atmospheric holes are observed to move in the west-to-east direction. This motion implies that their azimuthal speed around the Sun at 1 AU is less than Earth's orbital speed. As *Frank et al.* [1986*g*] point out, such azimuthal speeds can be accounted for by prograde orbits with perihelia somewhat inside Earth's orbit and moderate inclinations, for example, perihelia at 0.8 AU, aphelia at Jupiter's orbit or beyond, and an inclination of 35°.

Dessler [1991, p. 378] notes that the "diurnal variations in small comet event rate are unlike any of the radio-meteor observations [*Chubb,* 1986]." The diurnal variations of the rates of atmospheric holes as given in the first paper by *Frank et al.* [1986*a*] are shown in Figure 14. Of course, atmospheric hole rates cannot be determined for nighttime. The meteor rates from a ground-based, backscatter radar station are also shown in Figure 14 for an appropriate latitude [*Keay and Ellyett,* 1969]. The diurnal variations as determined with forward scatter radar are similar [*Vogan and Campbell,* 1957]. The agreement between the diurnal variations for atmospheric holes and radar meteors is obviously good.

Frank et al. [1987*a*] are able to determine the temporal variations of the atmospheric hole rates for a fixed area of dayglow. This area, 1.1 x 10^7 km², is bounded by Earth-centered solar-ecliptic latitudes 30° $\leq \theta_{SE} \leq$ 90° and longitudes 285° $\leq \phi_{SE} \leq$ 315°. The temporal variations of atmospheric hole rates for the period November 1, 1981, through January 21, 1982, in 2-day intervals are shown in the top panel of Figure 15. The averaged, daily meteor rates as determined with forward scatter radar from the same days but for a different year are shown in the bottom panel of Figure 15 [*Vogan and Campbell,* 1957]. We assume that the radar meteor rates are qualitatively similar from year to year. Periods of major showers are indicated by open circles and by closed circles for the nonshower periods. No evidence of increases of atmospheric hole rates during radar meteor showers are found in the figure. Instead, there is a remarkable correlation of the atmospheric hole rates with the nonshower, or sporadic, radar meteor rates. In the paper by *Frank et al.* [1987*a*] the latter rate for November 30, 1955, is plotted incorrectly D.I. Steele and S. V. M. Clube, private communication, 1991) and is correctly shown in Figure 15. The reader should note the remarkable correlations between the atmospheric hole rates and the nonshower radar-meteor rates shown in Figure 15, for example, (1) the overall decrease in meteor rates by a factor of ~10 over the period November 1 to mid-January, (2) the decrease in rates on ~November 8, (3) the increase in rates on ~November 30, (4) the period of more or less constant rates during ~December 20 to January 6, and (5) the minimum in event rates in mid-January

with subsequent recovery,

Dessler [1991] miscites the above forward scatter radar measurements as backscatter radar measurements. This is an important point. The weakly bound small comets and mantle debris are expected to produce ionization at higher altitudes relative to that from stony or iron meteoroids. Forward scatter radar is much more sensitive to ionization at higher altitudes relative to backscatter radar stations [cf. *McKinley*, 1961]. Thus the correlation of atmospheric hole rates with those of radar meteors is expected in forward scatter, whereas backscatter radar events are dominated by the infall of iron and stony meteoroids.

Dessler [1991] suggests that the temporal variations of atmospheric hole rates shown in the top panel of Figure 15 are due to varying views of the area in response to changes of the line of apsides and local time of the spacecraft orbit. That is, the atmospheric hole rates are proportional to the number of pixels within the dayglow area as a function of time. The line of apsides and local time vary slowly for the orbit of Dynamics Explorer 1. The rate of precession of the line of apsides is 0.328°/d, and the local time of the plane of the polar orbit changes at the rate of ~ - 4 min/d. Thus the rapid increases and decreases in atmospheric hole rates cannot be accounted for by changes in the viewing of the dayglow area. On November 1, 1981, apogee is located at 72.3° N and the orbital geographic local time is 0819 LT. On January 21, 1982, these orbital parameters are 45.2° N and 0231 LT, respectively. Thus the number of pixels for an image of the selected area increases slowly with time during this period. If the atmospheric holes are due to an instrumental artifact, then the rates shown in Figure 15 are expected to increase over the observing period in contrast to the overall decline by a factor of ~10.

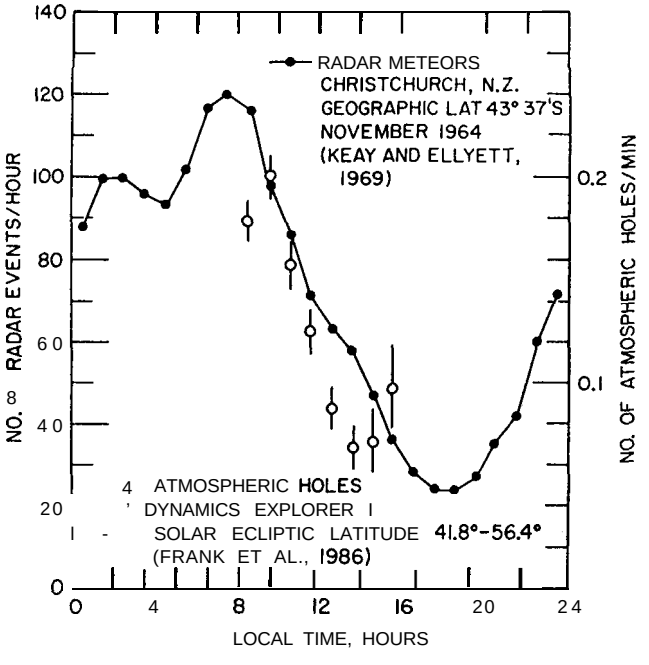

Figure 14. Comparison of the diurnal variations of the rates of atmospheric holes and radar meteors at mid-latitudes. The occurrence rates for atmospheric holes are given for an area of 1.8 x 10^6 km².

Chubb [1986] notes that if the atmospheric holes are not an instrumental artifact, then the pixels in a scan line that are adjacent to the darkened pixel should exhibit some intensity decrease on the average due to pixel overlap. Consideration of Figure 13 provides insight into this anticipated effect. Cragin et al. [1987] give a quantitative analysis that yields the average expected decrease in responses in these adjacent pixels, ~ -9%. *Frank et al.* [1987*b*] extend these statistical analyses to include the observations of a region of emissions associated with the atmospheric holes (see Plate 1 and Figure 13). The observed distributions of pixel counts are well fit by an object characterized by the opaque disk with a bright half-limb as shown in Figure 13. The average decreases in responses for the two pixels adjacent to the darkened pixel are then expected to be ~ - 2.3%. The observed decreases are - 1.4 (±0.4)% and within agreement with the expected value in consideration of the oversimplified model. *Sigwarth* [1988] provides quantitative estimates of the ultraviolet emissions from the impact of the cometary gases with atmospheric oxygen atoms and ions at altitudes below ~1000 km. These intensities are sufficient to account for the luminous feature observed in association with the atmospheric hole.

The bright feature associated with an atmospheric hole is of significantly lesser statistical significance than the decreases of ultraviolet intensities within the atmospheric holes [*Frank et al.*, 1987*b*]. Identification of this bright feature in the Viking images of atmospheric holes is not possible because of the limited number of dayglow images and the levels of electronic noise and statistical fluctuations in the sensor responses [*Frank et al.*, 1989].

As first noted by *Chubb* [1986] and presently by *Dessler* [1991]. the apparent size of the atmospheric hole as viewed by Dynamics Explorer 1 must increase as the spacecraft approaches Earth during its Perigee crossings. *Frank et al.* [1986*g*] find some evidence of increases in apparent size of the atmospheric holes when the spacecraft approaches Earth that is generally considered inconclusive. After further analysis we find that background counting rates due to penetrating charged particles in the inner radiation zone preclude detection of atmospheric holes at the lower altitudes with the exception of very selected viewing situations. The photometer is provided with a special tantalum shield with thickness 1.3 g/cm², excluding the acceptance area of the photocathode. The tantalum shield is penetrated by protons ≳ 30 MeV and electrons ≳ 5 MeV. The omnidirectional geometric factor for the detection of electrons ≳ 5 MeV is estimated to be ~0.01 cm² on the basis of photometer responses when viewing away from Earth. Intensities of electrons ≳ 5 MeV arc ~10^5, 10^6, and 10^7 cm^{-2} s^{-1} at geocentric radial distances ~2.5, 1.5, and 1.2 R_E along the magnetic equatorial plane [cf. *McIlwain*, 1963]. The spatial distribution is characterized by a latitudinal extent of ~± 30". The corresponding pixel responses for the above electron intensities are ~3,30, and 300 counts/pixel, respectively.

Because dayglow responses are ~30 to 50 counts/pixel it

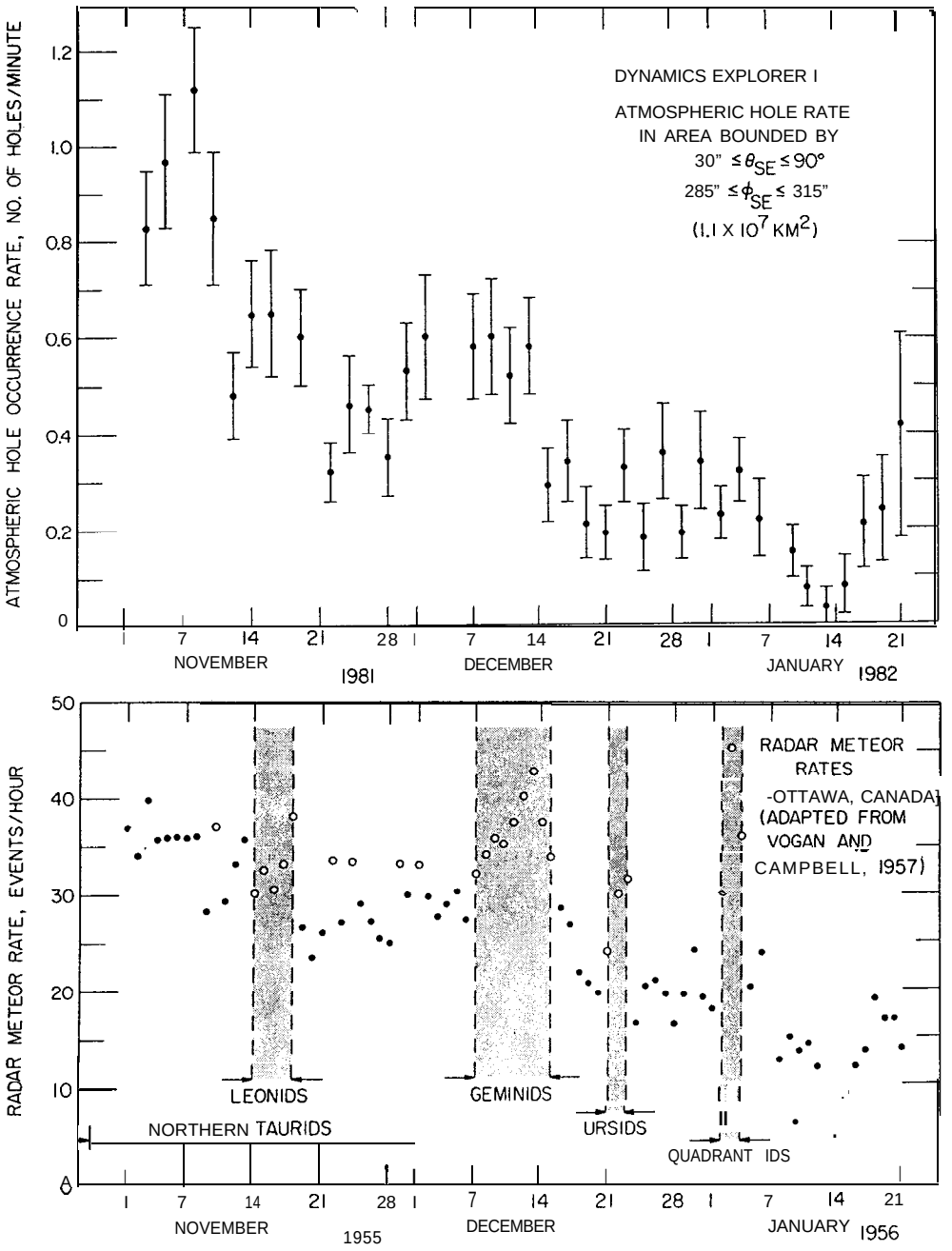

Figure 15. (Upper panel) Average occurrence rates of atmospheric holes during the period November 1981 through late-January 1982. (Lower panel) Forward scatter meteor rates reported by *Vogan and Campbell* [1957] for the same months but for earlier years 195.5 and 1956 [after *Frank et al.*, 1987*a*].

is clear that the detection of atmospheric holes is not generally possible if the background due to energetic electrons is 10 to 20 counts/pixel or more, i.e., at altitudes $\lesssim 1\ R_e$. At higher altitudes the energetic electron background also affects the statistical analysis. Although not noted by *Cragin et al.* [1987] their analysis shows that event rates for hole depths of $\sim 5.0\sigma$ to 6.4σ decreases with decreasing altitude for the two altitude bins $h > 19{,}500$ km and $12{,}600 < h < 19{,}500$ km by a factor of ~1.7 (see their Figure 1). This result is in contradiction to the greater decreases expected as the spacecraft approaches the cometary water clouds but is easily accounted for by increasing background rates due to penetrating electrons. Thus not only is the search for atmospheric holes hampered by the limited imaging time available at low altitudes because of the eccentric orbit of the spacecraft, the background rates from energetic electrons in the inner radiation zone further severely restrict the viewing geometries for the detection of atmospheric holes.

A few images of the dayglow as taken from low altitudes and with sufficiently low background rates for detection of atmospheric holes are available. Two examples of atmospheric holes in this severely limited data set are shown in Figure 16. The reader is reminded that a range of sizes for atmospheric holes should be detected at these altitudes be-

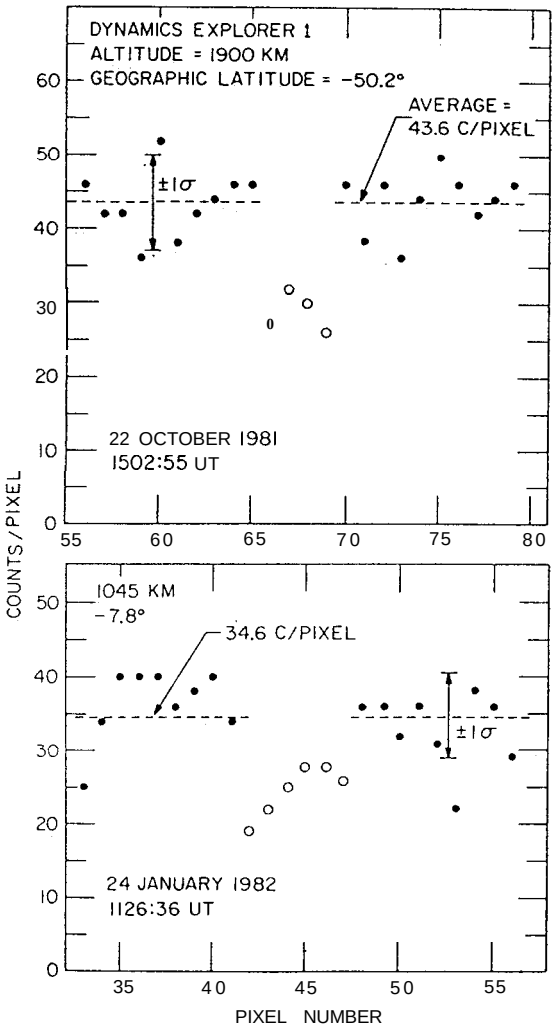

Figure 16. 'ho examples of strings of darkened pixels in a scan line due to the cometary water clouds as viewed at low altitudes with the imaging photometer on Dynamics Explorer 1.

cause the cometary water clouds are expanding after disruption at ~1000 km (see section 2.2.2). Of course, at low altitudes, only a small fraction of the dayglow area is viewed. The cometary water clouds are detected in only one scan line because their apparent angular motion at these altitudes is large relative to the angular motion of the scanning mirror in the spin-scan photometer [*Frank et al.* 1986*g*]. For the event on October 22, 1981, the probability that the string of four adjacent darkened pixels is a random event is ~1.4 x 10^{-3} in the entire data set ~3 x 10^{4} pixels. This probability for the string of six adjacent darkened pixels on January 24, 1982, is ~2 x 10^{-4}. Thus, with consideration of the background responses due to energetic electrons in the inner zone, the expected strings of darkened pixels at low altitudes are identified.

The maximum spatial dimensions are determined by the line-of-sight distances from the spacecraft to an altitude of 300 km. These line-of-sight distances are 1605 and 755 km for October 22 and January 24, respectively, and the corresponding object diameters are 26 and 18 km, respectively. If the cometary water clouds are closer to the spacecraft, the dimensions are similarly decreased.

The preferred east-to-west motion of the atmospheric holes across the sunlit face of Earth, the diurnal variations of occurrence rates, the temporal variations of these rates, and the larger apparent angular sizes at low altitudes establish atmospheric holes as a geophysical phenomenon, and not an instrumental artifact.

7. SUMMARY

From the discussion of the preceding section it should be apparent to the reader that an instrumentation artifact cannot account for (1) the predominantly east-to-west motion of the atmospheric holes, (2) the correlation of the diurnal variations of occurrence rates of atmospheric holes with those of radar meteors, (3) the correlation of the temporal variations of the atmospheric hole rates with the nonshower meteor rates detected with forward scatter radar, and (4) the sightings of atmospheric holes with large apparent angular sizes at low altitudes. Atmospheric holes with similar dimensions and occurrence frequencies are found in the limited number of ultraviolet dayglow images available from the Viking spacecraft. Two entirely different observational techniques confirm the existence of the small comets and yield fluxes and masses that are in coarse agreement with the inferred values from the observations of atmospheric holes with Dynamics Explorer I, i.e., sightings of small comets with a ground-based telescope and detection of water bursts in the upper atmosphere with a microwave radiometer.

Much of the debate concerning the geophysical, lunar, and interplanetary effects of the presence of a small-comet swarm in the inner solar system arises from a general lack of adequate modeling or of knowledge of the physical characteristics of the small comets. Examples include (1) the impact of a water cloud with Earth's upper atmosphere, (2) the visual magnitude of the luminosity of the expanding water cloud from disruption of the small comet, (3) the seismic wave amplitude and surface deformation from small-comet impacts on the loose soil of the Moon, and (4) the composition and the mechanical nature of the mantles of the small comets. It is our conclusion from our rudimentary analyses of these problems that the small comets can be accommodated if they exist.

The next several years promise to be exciting in the resolution of the small-comet controversy. A search for transient light bursts from small-comet impacts on the Moon is currently underway. Amateur astronomers are adequately equipped to corroborate the first ground-based telescopic detection of the small comets. The searches for cometary water vapor in the inner solar system, an extended lunar atmosphere from cometary impacts, and a cometary tail from near-misses of small comets with Earth's atmosphere are being accomplished with the ultraviolet spectrometer on the Galileo spacecraft. In 1994 the Earth's ultraviolet dayglow is to be revisited by cameras capable of significantly im-

proved temporal and spatial resolution when they are launched on the Polar spacecraft of the International Solar Terrestrial Physics Mission.

7.1. Some Personal Reflections

Our personal reflections are appropriately discussed in the trade book by *Frank* [1990] now available in English and Japanese.

Acknowledgments. The authors are greatly indebted to J. J. Olivero for the use of his mesospheric water measurements with a microwave radiometer, L. H. Brace for his data for ionospheric densities from Dynamics Explorer 2, and A. L. Lane for his suggestions concerning the possibility of ultraviolet dayglow absorption by cometary water dimers and clusters. We are also grateful for useful discussions with R. A. heelis and C. W. Hord and for constructive comments from the editor, M. Neugebauer, and the three reviewers. This research is supported in part by NASA under grants NAG5-483 and NAGW-1631. This paper is dedicated to the memory of Clayne M. Yeates, who designed and successfully completed the first ground-based telescopic search for small comets.

M. Neugebauer was the Editor responsible for this paper. She thanks three anonymous referees for their assistance in evaluating this paper.

References

Adams, D. M., Extreme short-term variability in upper atmospheric water vapor as measured by ground-based microwave radiometry, M. S. thesis, Pa. State Univ., University Park, 1988.

Adams, D. M., J. J. Olivero, and C. L. Croskey, A search for extraterrestrial water in the upper atmosphere by ground-based microwave radiometry (abstract), *Eos Trans. AGU, 68,* 372, 1987.

Ajello, J. M., A. I. Stewart, G. E. Thomas, and A. Graps, Solar cycle study of interplanetary Lyman-alpha variations: Pioneer Venus Orbiter sky background results, *Astrophys. J., 317,* 964-986, 1987.

Anderson, D. E. Jr., R. R. Meier, P. D. Feldman, and E. P. Gentieu, The UV dayglow 3, 01 emissions at 989, 1027, 1152, 1304, and 1356A, *Geophys. Res. Lett., 7,* 1057-1060, 1980.

Bailey, G. J., and R. A. Heelis, Ion temperature troughs induced by a meridional neutral air wind in the night-time equatorial topside ionosphere, *Planet. Space Sci., 28,* 895-906, 1980.

Baker, D. A., and J. E. Hammel, Experimental studies of the penetration of a plasma stream into a transverse magnetic field, *Phys. Fluids, 8,* 713-722, 1965.

Baldwin, R. B., On the current rate of formation of impact craters of varying sizes on the Earth and Moon, *Geophys. Res. Lett., 14,* 216-219, 1987.

Banks, l? M., A new means for observation of small comets and other water-laden bodies entering Earth's upper atmosphere, *Geophys. Res. Lett., 16,* 575-578, 1989.

Banks, P. M., and G. Kockarts, *Aeronomy, Part A,* p. 13, Academic, San Diego, Calif., 1973.

Barney, G. O., and J. C. Sprott, Double vortex flows in plasmas axially traversing multipole magnetic fields, *Phys. Fluids, 12,* 707-712, 1969.

Berry, R. S., Structure and dynamics of clusters: An introduction, in *The Chemical Physics of Atomic and Molecular Clusters,* edited by G. Scoles, pp. 3-22, North-Holland, New York, 1990.

Bevilacqua, R. M., J. J. Olivero, I? R. Schwartz, C. J. Gibbins, J. M. Bologna, and D. L. Thacker, An observational study of water vapor in the mid-latitude mesosphere using ground-based microwave techniques, *J. Geophys. Res., 88,* 8523-8534, 1983.

Bevilacqua, R. M., M. Allen, D. F. Strobel, M. E. Summers, and J. J. Olivero, The seasonal variation of water vapor and ozone in the upper mesosphere: Implications for vertical transport and ozone photochemistry, *J. Geophys. Res., 95,* 883-893, 1990.

Bonadonna, M. F., A search for episodic increases in upper atmospheric water vapor as evidence of an extraterrestrial source, M. S. thesis, Pa. State Univ., University Park, 1990.

Bonadonna, M. F., J. J. Olivero, and C. L. Croskey, In search of small comets: H_2O bursts observed in the mesosphere (abstract), *Eos Trans. AGU, 71,* 570, 1990.

Brasseur, G., and S. Solomon, *Aeronomy of the Middle Atmosphere,* D. Reidel, Hingham, Mass., 1984.

Brin, G. D., and D. A. Mendis, Dust release and mantle development in comets, *Ap. J., 229,* 402-408, 1979.

Bronshten, V. A., *Physics of Meteoric Phenomena,* D. Reidel, Hingham, Mass., 1983.

Chubb, T. A., Comment on the paper "On the influx of small comets into the Earth's upper atmosphere I. Observations," *Geophys. Res. Lett., 13,* 1075-1077, 1986.

Cragin, B. L., Comment on "Search for atmospheric holes with the Viking cameras" by Frank et al., *Geophys. Res. Lett., 17,* 1173-1174, 1990.

Cragin, B. L., W. B. Hanson, R. R. Hodges, and D. Zuccaro, Comment on the papers "On the influx of small comets into the Earth's upper atmosphere, I. Observations and II. Interpretation," *Geophys. Res. Lett., 14,* 573-576, 1987.

Davis, P. M., Comment on the letter "On the influx of small comets into the Earth's upper atmosphere," *Geophys. Res. Lett., 13,* 1181-1183, 1986.

Delsemme, A. H., Chemical composition of cometary nuclei, in *Comets,* edited by L. L. Wilkening, pp. 85-130, University of Arizona Press, Tucson, 1982.

Delsemme, A. H., and D. C. Miller, Physico-chemical phenomena in comets, *Planet. Space Sci., 19,* 1229-1257, 1971.

Dessler, A. J., The small-comet hypothesis, *Rev. Geophys., 29,* 355-382, 1991.

Dessler, A. J., B. R. Sandel, and V. M. Vasyliunas, Terrestrial cometary tail and lunar corona induced by small comets: Predictions for Galileo, *Geophys. Res. Lett., 17,* 2257-2260, 1990.

Donahue, T. M., Comment on the paper "On the influx of small comets into the Earth's upper atmosphere, II. Interpretation" by L. A. Frank, J. B. Sigwarth and J. D. Craven, *Geophys. Res. Lett., 13,* 555-557, 1986.

Donahue, T. M., Small comets: Implications for interplanetary Lyman-alpha, *Geophys. Res. Lett., 14,* 213-215, 1987

Donahue, T. M., T. I. Gombosi, and B. R. Sandel, Cometesimals in the inner solar system, *Nature, 330,* 548-550, 1987.

Dorsey, N. E., *Properties of Ordinary Water Substanc,* Reinhold, New York, 1940.

Dyke, T. R., and J. S. Muenter, Molecular beam electric deflection studies of water polymers, *J. Chem. Phys., 57,* 5011-5012, 1972.

Dyke, T. R., K. M. Mack, and J. S. Muenter, The structure of water dimer from molecular beam resonance spectroscopy, *J. Chem. Phys., 66,* 498-510, 1977.

Everhart, E., Change in total energy of comets passing through the solar system, *Astron. J., 73,* 1039-1052, 1968.

Everhart, E., Close encounters of comets and planets, *Astron. J., 74,* 735-750, 1969.

Everhart, E., The evolution of comet origins as perturbed by Uranus and Neptune, in *Comets, Asteroids, Meteorites: Interrelations, Evolutions and Origins,* edited by A. H. Delsemme, pp. 99-104, University of Toledo Press, Toledo, Ohio, 1977.

Fanale, F. P., and J. R. Salvail, An idealized short-period comet model: Surface insolation, H_2O flux, dust flux, and mantle evolution, *Icarus, 60,* 476-511, 1984.

Fastie, W. G., P. D. Feldman, R. C. Henry, H. W. Moos, C. A. Barth, G. E. Thomas, and T. M. Donahue, A search for far-ultraviolet emissions from the lunar atmosphere, *Science, 182,* 710-711, 1973.

Feldman, P. D., and D. Morrison, The Apollo 17 ultraviolet spectrometer: Lunar atmosphere measurements revisited, *Geophys. Res. Lett., 18,* 2105-2108, 1991.

Fernández, J. A., On the existence of a comet belt beyond Neptune, Mon. *Not. R. Astron. Soc., 192,* 481-491, 1980.

Frank, L. A., Atmospheric holes and the small comet hypothesis, *Aust. Phys., 26,* 19-34, 1989.

Frank, L. A. (with Patrick Huyghe), *The Big Splash,* Birch Lane, New York, 1990. (Reprinted by Avon, New York, 1991.)

Frank, L. A., and J. D. Craven, Imaging results from Dynamics Explorer 1, *Rev. Geophys., 26,* 249-283, 1988.

Frank, L. A., J. D. Craven, K. L. Ackerson, M. R. English, R. H. Eather, and R. L. Carovillano, Global auroral imaging instrumentation for the Dynamics Explorer Mission, *Space Sci. Instrum., 5,* 369-393, 1981.

Frank, L. A., J. B. Sigwarth, and J. D. Craven, On the influx of small comets into the Earth's upper atmosphere, I, Observations, *Geophys. Res. Lett., 13,* 303-306, 1986*a*.

Frank, L. A., J. B. Sigwarth, and J. D. Craven, On the influx of small comets into the Earth's upper atmosphere, II, Interpretation, *Geophys. Res. Lett., 13,* 307-310, 1986*b*.

Frank, L. A., J. B. Sigwarth, and J. D. Craven, Reply, *Geophys. Res. Lett., 13,* 559-560, 1986*c*.

Frank, L. A., J. B. Sigwarth, and J. D. Craven, Reply, *Geophys. Res. Lett., 13,* 703-704, 1986*d*.

Frank, L. A., J. B. Sigwarth, and J. D. Craven, Reply, *Geophys. Res. Lett., 13,* 979-980, 1986*e*.

Frank, L. A., J. B. Sigwarth, and J. D. Craven, Reply, *Geophys. Res. Lett., 13,* 985-988, 1986*f*.

Frank, L. A., J. B. Sigwarth, and J. D. Craven, Reply, *Geophys. Res. Lett., 13,* 1079-1082, 1986*g*.

Frank, L. A., J. B. Sigwarth, and J. D. Craven, Reply to Davis and Nakamura et al., *Geophys. Res. Lett., 13,* 1186-1189, 1986*h*.

Frank, L. A., J. B. Sigwarth, and J. D. Craven, Reply to Morris, *Geophys. Res. Lett., 13,* 1484-1486, 1986*i*.

Frank, L. A., J. B. Sigwarth, and J. D. Craven, Reply to Soter, *Geophys. Res. Lett., 14,* 164-167, 1987*a*.

Frank, L. A., J. B. Sigwarth, and J. D. Craven, Reply to Cragin et al., *Geophys. Res. Lett., 14,* 577-580, 1987*b*.

Frank, L. A., J. B. Sigwarth, and J. D. Craven, Reply to Wasson and Kyte, *Geophys. Res. Lett., 14,* 781-782, 1987*c*.

Frank, L. A., J. B. Sigwarth, and J. D. Craven, Search for atmospheric holes with the Viking cameras, *Geophys. Res. Lett., 16,* 1457-1460, 1989.

Frank, L. A., J. B. Sigwarth, and J. D. Craven, Reply, *Geophys. Res. Lett., 17,* 1175-1176, 1990*a*.

Frank, L. A., J. B. Sigwarth, and C. M. Yeates, A search for small solar-system bodies near the Earth using a ground-based telescope: Technique and observations, *Astron. Astrophys., 228,* 522-530, 1990*b*.

Garcia, R. R., and S. Solomon, A numerical model of the zonally averaged dynamical and chemical structure of the middle atmosphere, *J. Geophys. Res., 88,* 1379-1400, 1983.

Garrett, H. B., The charging of spacecraft surfaces, *Rev. Geophys., 19,* 577-616, 1981.

Gehrels, T., and F. Vilas, A CCD search for geosynchronous debris, *Icarus, 68,* 412-417, 1986.

Gehrels, T., B. G. Marsden, R. S. McMillan, and J. V. Scotti, Astrometry with a scanning CCD, *Astron. J., 91,* 1242-1243, 1986.

Hall, D. T., and D. E. Shemansky, The evidence against an inner solar system source of atomic hydrogen, *Bull. Am. Astron. Soc., 20,* 836, 1988a.

Hall, D. T., and D. E. Shemansky, No cometesimals in the inner solar system, *Nature, 335,* 417-419, 19886.

Hansen, J. E., and L. D. Travis, Light scattering in planetary atmospheres, *Space Sci. Rev., 16,* 527-610, 1974.

Hanson, W. B., Comment, *Geophys. Res. Lett., 13,* 981-984, 1986.

Harnwell, G. P., *Principles of Electricity and Electromagnetism,* problem 12, p. 79, McGraw-Hill, New York, 1949.

Hills, J. G., Comet showers and the steady-state infall of comets from the Oort cloud, *Astron. J., 86,* 1730-1740, 1981.

Holland, H. D., *The Chemical Evolution of the Atmosphere and Oceans,* Princeton University Press, Princeton, N. J., 1984.

Holsapple, K. A., and R. M. Schmidt, On the scaling of crater dimensions, 2. Impact processes, *J. Geophys. Res., 87,* 1849-1870, 1982.

Hord, C. W., et al., Galileo ultraviolet spectrometer experiment, *Space Sci. Rev., 60* (1-4), 503-530, 1992.

Horwitz, J. L., R. H. Comfort, and C. R. Chappell, A statistical characterization of plasmasphere density structure and boundary locations, *J. Geophys. Res., 95,* 7937-7947, 1990.

Hunten, D. M., and T. M. Donahue, Hydrogen loss from the terrestrial planets, *Annu. Rev. Earth Planet. Sci., 4,* 265-292, 1976.

Jacchia, L. G., Thermospheric temperature, density, and composition: New models, *SAO Spec. Rep. 375,* Astrophys. Observ., Smithsonian Inst., Cambridge, Mass., 1977.

Johnson, R. E., J. E Cooper, and L. J. Lanzerotti, Radiation formation of a non-volatile crust, Proceedings of the 20th ESLAB Symposium on the Exploration of Comet Halley, *Eur. Space Agency Spec. Publ., ESA SP-250,* 269-272, 1986.

Keay, C. S. L., and C. D. Ellyett, Southern hemisphere meteor rates, *Mem. R. Astron. Soc., 72,* 185-232, 1969.

Keller, H. U., et al., First Halley multicolour camera imaging results from Giotto, *Nature, 321,* 320-326, 1986.

Kolovos, G., J. H. Seimdakis, H. Varvoglis, and S. Avgoloupis, Photographic evidence of a short duration: Strong flash from the surface of the Moon, *Icarus, 76,* 525-532, 1988.

Lämmerzahl, P., et al., Expansion velocity and temperatures of gas and ions measured in the coma of comet P/Halley, *Astron. Astrophys., 187,* 169-173, 1987.

Lanzerotti, L. J., W. L. Brown, and R. E. Johnson, Laboratory studies of ion irradiations of water, sulfur dioxide, and methane ices, in *Ices in the Solar System,* edited by J. Klinger, D. Benest, A. Dollfus, and R. Smoluchowski, pp. 317-335, D. Reidel, Hingham, Mass., 1985.

Latham, G., M. Ewing, F. Press, G. Sutton, J. Dorman, Y. Nakamura, N. Toksöz, D. Lammlein, and F. Duennebier, Passive seismic experiment, Apollo 16 Preliminary Science Report, *NASA Spec. Publ., SP-315,* (9)1-(9)29, 1972.

Latham, G., M. Ewing, J. Dot-man, Y. Nakamura, E Press, N. Toksöz, G. Sutton, F. Duennebier, and D. Lammlein, Lunar structure and dynamics-Results from the Apollo passive seismic experiment, *Moon, 7,* 396-420, 1973.

Liou, K.-N., *An Introduction to Atmospheric Radiation,* Academic, San Diego, Calif., 1980.

Lumme, K., and E. Bowell, Radiative transfer in the surfaces of the atmosphereless bodies, I, Theory, *Astron. J., 86,* 1694-1704, 1981*a*.

Lumme, K., and E. Bowell, Radiative transfer in the surfaces of the atmosphereless bodies, II, Interpretation of phase curves, *Astron. J., 86,* 1705-1721, 1981*b*.

McIlwain, C. E., The radiation belts, natural and artifical, *Science, 142,* 355-361, 1963.

McKay, C. P., Comment, *Geophys. Res. Lett., 13,* 976-978, 1986.

McKinley, D. W. R., *Meteor Science and Engineering,* McGraw-Hill, New York, 1961.

Meier, R. R., Issues relating to "holes" in the 01 1304 Å far U.V. dayglow, *Planet. Space Sci., 35,* 1297-1299, 1987.

Meier, R. R., and H. U. Keller, Predictions of the hydrogen Lyman *a* coma of Comet Halley, *Icarus, 62,* 521-537, 1985.

Meier, R. R., D. J. Strickland, P. D. Feldman, and E. P. Gentieu, The ultraviolet dayglow, 1, Far UV emission of N and N_2, J. *Geophys. Res., 85,* 2177-2184, 1980.

Mendillo, M., J. B. Sigwarth, J. D. Craven, L. A. Frank, J. Holt, and D. Tetenbaum, Project ERIC: The search for environmental reactions induced by comets, *Adv. Space Res., 10,* (7)83-(7)87, 1990.

Morgan, T. H., and D. E. Shemansky, Limits to the lunar atmosphere, *J. Geophys. Res., 96,* 1351-1367, 1991.

Morris, D. E., Comment on "On the influx of small comets into the Earth's upper atmosphere II. Interpretation," *Geophys. Res. Lett., 13,* 1482-1483, 1986.

Murad, E., and P. Bochsler, Spectulations about the origin of H_3O^+ seen in cometary mass spectra, *Nature, 326,* 366-367, 1987.

Mutel, R. L., J. D. Fix, and D. V. Deleo, A detection experiment for small comet lunar impacts, internal report, Univ. of Iowa, Iowa City, 1991.

Nakamura, Y., J. Oberst, S. Clifford, and B. Bills, Comment on the letter "On the influx of small comets into the Earth's upper atmosphere, II. Interpretation," *Geophys. Res. Lett., 11,* 1184-1185, 1986.

Newton, H. A., On the capture of comets by planets, especially their capture by Jupiter, *Mem. Natl. Acad. Sci., 6,* 7-23, 1893.

Odutola, J. A., and T. R. Dyke, Partially deuterated water dimers: Microwave spectra and structure, *J. Chem. Phys., 72,* 5062-5070, 1980.

O'Keefe, J. D., and T. J. Ahrens, Cometary and meteorite swarm impact on planetary surfaces, *J. Geophys. Res., 87,* 6668-6680, 1982.

Oort, J. H., The structure of the cloud of comets surrounding the solar system, and a hypothesis concerning its origin, *Bull. Astron. Inst. Neth., 11,* 91-110, 1950.

Opal, C. B., and G. R. Carruthers, Lyman-a observations of Comet West (1975n), *Icarus, 31,* 503-509, 1977.

Öpik, E. J., *Physics of Meteor Flight in the Atmosphere,* Wiley-Interscience, New York, 1958.

Pike, C. P., et al., Release of liquid water from the Space Shuttle, *Geophys. Res. Lett., 17,* 139-142, 1990.

Reid, G. C., and S. Solomon, On the existence of an extraterrestrial source of water vapor in the middle atmosphere, *Geophys. Res. Lett.,* 13, 1129-1131, 1986.

Rozenberg, G. V., *Twilight, A Study in Atmospheric Optics,* Plenum, New York, 1966.

Schmidt, G., Plasma motion across magnetic fields, *Phys. Fluids, 3,* 961-965, 1960.

Shardanand, Experimental evidence for Xe_2 molecules, *Phys. Rev., 160,* 67-71, 1967.

Sigwarth, J. B., Imaging of absorption and emission features of water-vapor clouds associated with small comets as observed with Dynamics Explorer 1, M.S. thesis, Univ. of Iowa, Iowa City, 1988.

Sigwarth, J. B., A search for small comets in consecutive images acquired with a ground-based telescope, Ph.D. thesis, Univ. of Iowa, Iowa City, 1989.

Solomon, S., E. E. Ferguson, D. W. Fahey, and P. J. Crutzen, On the chemistry of H_2O, H_2 and meteoritic ions in the mesosphere and lower thermosphere, *Planer. Space Sci., 30,* 1117-1126, 1982.

Soter, S., Comment on the paper "On the influx of small comets into the Earth's upper atmosphere," *Geophys. Res. Lett., 14,* 162-163, 1987.

Stewart, A. I. F., B. M. Jakosky, G. R. Gladstone, and R. T. Clancy, Small comets and atmospheric holes: Do they exist? (abstract), *Eos Trans. AGU, 67,* 565, 1986.

Storrs, A. D., F. P. Fanale, R. S. Saunders, and J. B. Stephens, The formation of filamentary sublimate residues (FSR) from mineral grains, *Icarus, 76,* 493-512, 1988.

Taff, L. G., Satellite debris: Recent measurements, *J. Spacecraft, 23,* 342-346, 1986.

Tsou, J. J., Microwave radiometric measurements of mesospheric water vapor: Ground-based observations in both solar absorption and atmospheric emission modes, Ph.D. thesis, Pa. State Univ., University Park, 1986.

van de Hulst, H. C., *Light Scattering by Small Particles,* John Wiley, New York, 1957.

Vogan, E. L., and L. L. Campbell, Meteor signal rates observed in forward-scatter, *Can. J. Phys., 35,* 1176-1189, 1957.

Watanabe, K., and M. Zelikoff, Absorption coefficients of water vapor in the vacuum ultraviolet, *J. Opt. Soc. Am., 43,* 753-755, 1953.

Yeates, C. M., Initial findings from a telescopic search for small comets near Earth, *Planer. Space Sci., 37,* 1185-1196, 1989.

Zel'dovich, Ya. B., and Yu. P. Raizer, *Physics of Shock Waves and High-Temperature Hydrodynamic Phenomena,* vol. II, edited by W. D. Hayes and R. F. Probstein, Academic, San Diego, Calif., 1967.

L. A. Frank and J. B. Sigwarth, Department of Physics and Astronomy, University of Iowa, Iowa City, IA 52242.